Article

In vitro reconstitution of meiotic DNA double-strand-break formation

https://doi.org/10.1038/s41586-024-08551-1

Received: 2 September 2024

Accepted: 19 December 2024

Published online: 19 February 2025

Open access

Check for updates

Xinzhe Tang[1,5], Zetao Hu[2,3,5], Jian Ding[1], Meixia Wu[1], Pin Guan[1], Yawei Song[1], Yue Yin[4], Wei Wu[1], Jinbiao Ma[3], Ying Huang[2]✉ & Ming-Han Tong[1]✉

The Spo11 complex catalyses the formation of DNA double-strand breaks (DSBs), initiating meiotic recombination—a process that is essential for fertility and genetic diversity[1,2]. Although the function of Spo11 has been known for 27 years, previous efforts to reconstitute DSB formation in vitro have been unsuccessful. Here we biochemically characterize the mouse SPO11–TOP6BL protein complex, and show that this complex cleaves DNA and covalently attaches to the 5′ terminus of DNA breaks in vitro. Using a point-mutation strategy, we reveal that Mg^{2+} is essential for the DNA-cleavage activity of this complex in vitro, as confirmed by knock-in mice carrying a point mutation in SPO11 that disrupts its binding to Mg^{2+}, thereby abolishing DSB formation. However, the activity of the SPO11 complex is ATP-independent. We also present evidence that the mouse SPO11 complex is biochemically distinct from the ancestral topoisomerase VI. Our findings establish a mechanistic framework for understanding the first steps of meiotic recombination.

Meiosis is a fundamental biological process that generates haploid gametes from diploid progenitors in most sexually reproducing organisms, serving as the basis for sexual reproduction[3–5]. Homologous recombination, the most prominent feature of meiosis, enhances genetic diversity during inheritance, establishes physical connections between homologues to ensure precise segregation during prophase I of meiosis and keeps chromosome numbers stable within species[5,6]. This process is initiated by the programmed induction of DNA DSBs at hotspots, which is determined by PRDM9 in most mammals[7–11]. As early as 1997, using *Saccharomyces cerevisiae* as a model, it was known that meiotic DSBs are catalysed by Spo11, a widely conserved protein[1,2]. Subsequent studies in 2000, using mice, showed that SPO11 has a similar role in mammalian meiosis[12,13]. It was also well-known that SPO11 belongs to the DNA topoisomerase VI (topo VI) family, which are ATP/Mg^{2+}-dependent heterotetrameric type IIB topoisomerases composed of two Top6A and two Top6B subunits[1,2,14–16]. The activity of topo VI depends on the interaction between Top6A and Top6B subunits[1,14]. SPO11 shares extensive homology with the Top6A subunit, the catalytic subunit of the topo VI family[1,16–18]. The mouse orthologue of the Top6B subunit, TOP6BL (homologous to human C11orf80, also known as Gm960 in mice), which can interact with SPO11, was identified only in 2016[19,20]. It is well-established that, in vivo, a SPO11–TOP6BL complex is essential for the formation of meiotic DSBs[12,13,19,20].

Over the past 27 years, researchers have endeavoured to characterize the biochemical properties and structure of the Spo11 complex. Studies have shown the binding, in vitro, of *S. cerevisiae* Spo11 to DNA along with its partners Rec102, Rec104 and Ski8 (ref. 21). Moreover, the cryo-electron-microscopy structure of the yeast Spo11 core complex has been determined at up to 3.3 Å, although it remains incapable of cleaving DNA in vitro[22]. Despite these advances, how the SPO11 complex catalyses DNA cleavage, particularly in mammals, has remained unknown. In this study, together with the accompanying papers[23,24], we report the successful purification of the mouse SPO11–TOP6BL complex, presenting in vitro reconstitution of meiotic DSB formation.

Biochemical characterization of mouse SPO11–TOP6BL

Characterizing the biochemical properties of meiotic DSB machinery has been challenging, owing mainly to difficulties in purifying these complexes. We successfully expressed and purified N-terminally His-tagged mouse SPO11 (His–SPO11) and C-terminally Flag-tagged mouse TOP6BL (TOP6BL–Flag) proteins using Expi293F cells (Extended Data Fig. 1a,b). The resulting complex was characterized by size-exclusion chromatography (SEC), which exhibited a single peak with an estimated molecular mass of 118 kDa, calibrated against a protein standard (Fig. 1a,b). Given the individual molecular masses of SPO11 (44.6 kDa) and TOP6BL (63.8 kDa), these findings suggest that the complex forms a heterodimer with a 1:1 stoichiometry, yielding a calculated molecular mass of 108.4 kDa, which aligns closely with the SEC results. SDS–PAGE analysis further corroborated the heterodimeric nature of the complex, showing two distinct bands with an equal stoichiometric ratio (Fig. 1c). To enhance the stability and yield of the SPO11–TOP6BL complex, we purified the His–MBP–SPO11 (in which MBP is maltose-binding protein) and TOP6BL–Flag complex (Extended Data Fig. 1c). The His–MBP–SPO11 and TOP6BL–Flag complex also showed a single peak on SEC and exhibited two distinct bands on SDS–PAGE, consistent with the characteristics of the His–SPO11 and TOP6BL–Flag complex (Fig. 1c and Extended Data Fig. 1c). However, this

[1]Key Laboratory of Multi-Cell Systems, Shanghai Key Laboratory of Molecular Andrology, Shanghai Institute of Biochemistry and Cell Biology, Center for Excellence in Molecular Cell Science, Chinese Academy of Sciences, University of Chinese Academy of Sciences, Shanghai, China. [2]Shanghai Key Laboratory of Biliary Tract Disease Research, Department of General Surgery, Xinhua Hospital, Shanghai Jiao Tong University School of Medicine, Shanghai, China. [3]State Key Laboratory of Genetic Engineering, Collaborative Innovation Center of Genetics and Development, Department of Biochemistry and Biophysics, Institute of Plant Biology, School of Life Sciences, Fudan University, Shanghai, China. [4]National Facility for Protein Science in Shanghai, Shanghai Advanced Research Institute, Chinese Academy of Sciences, Shanghai, China. [5]These authors contributed equally: Xinzhe Tang, Zetao Hu. ✉e-mail: huangy@shsmu.edu.cn; minghan@sibcb.ac.cn

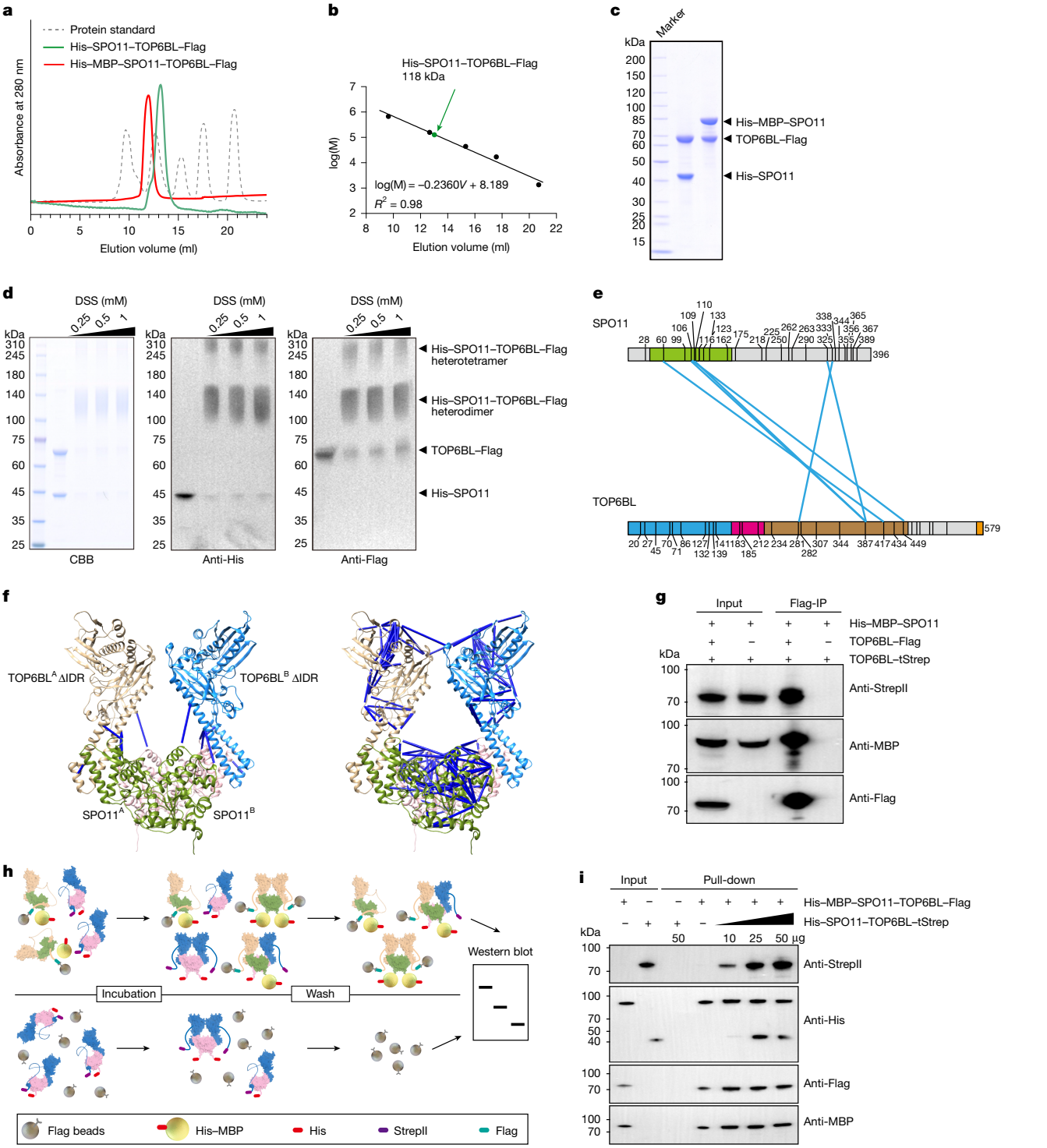

Fig. 1 | Biochemical characterization of the SPO11–TOP6BL complex. a, SEC elution profiles of the His–SPO11–TOP6BL–Flag (green) and His–MBP–SPO11–TOP6BL–Flag (red) complexes. The dashed line indicates the elution profile of protein standards. **b**, Calibration curve correlating protein standard retention times with molecular mass (M). The green dot indicates the retention time of SPO11–TOP6BL with its corresponding molecular mass. **c**, SDS–PAGE analysis showing the purity of the SPO11 and TOP6BL proteins ($n = 3$ independent experiments). **d**, Analysis of DSS-cross-linked samples by SDS–PAGE (left) and western blot using anti-His (middle) and anti-Flag (right) antibodies to detect His–SPO11 and TOP6BL–Flag, respectively ($n = 3$ independent experiments). CBB, Coomassie brilliant blue. **e**, Schematic representation of intermolecular cross-links between SPO11 and TOP6BL. **f**, Visualization of intermolecular cross-links (left) and cross-links at the SPO11–TOP6BL homo-interface (including intramolecular SPO11 or TOP6BL and intermolecular $SPO11^A$–$SPO11^B$ or $TOP6BL^A$–$TOP6BL^B$) (right) identified by cross-linking mass spectrometry (XL-MS). Only cross-links smaller than 30 Å are displayed using Xlinker in Chimera, on the basis of the AlphaFold 3-predicted structural model of SPO11–TOP6BL ΔIDR. **g**, Co-immunoprecipitation analysis showing Flag-immunoprecipitation (Flag-IP) detection of TOP6BL–Flag, His–SPO11, His–MBP–SPO11 (anti-His) and TOP6BL–tStrep (anti-StrepII) ($n = 3$ independent experiments). **h**, Schematic representation of the pull-down assay designed to detect SPO11–TOP6BL heterotetramer formation. **i**, Pull-down assay showing His–MBP–SPO11–TOP6BL–Flag interaction with His–SPO11–TOP6BL–tStrep, detected by anti-His, anti-MBP, anti-Flag and anti-Strep antibodies. Increasing the amount of His–SPO11–TOP6BL–tStrep resulted in a corresponding increase in the intensity of the pull-down bands, indicating enhanced binding with higher protein concentrations ($n = 3$ independent experiments).

observed stoichiometry differs from the 2:2 arrangement that would be expected on the basis of the ancestral complex, topo VI (refs. 14,25).

To further investigate the arrangement of the SPO11 complex, we conducted cross-linking experiments using disuccinimidyl suberate (DSS), followed by SDS–PAGE analysis. A band was observed at approximately 120 kDa, corresponding to the potential heterodimeric His–SPO11 and TOP6BL–Flag complex (Fig. 1d). Western blotting with His and Flag antibodies confirmed the presence of both tags in the approximately 120 kDa band, indicating the potential heterodimeric nature of the complex (Fig. 1d). Furthermore, a band at approximately 250 kDa containing both His and Flag signals was detected, suggesting a potential heterotetrameric assembly (Fig. 1d). SPO11 has 26 lysine residues, whereas TOP6BL has 28, with 6 located in the intrinsically disordered region (IDR) (Fig. 1e). To visualize the spatial relationship of these cross-links in the SPO11–TOP6BL complex, we generated structural predictions of the heterotetramer using AlphaFold 3. Owing to low accuracy in the predicted IDR positioning in full-length TOP6BL, as indicated by the predicted aligned error (PAE) diagram (Extended Data Fig. 2a,b), the tetramer structure was modelled for SPO11 and TOP6BL without the IDR region (Fig. 1f and Extended Data Fig. 2c,d). A total of 69 cross-links within DSS effective cross-linking distance (30 Å) was mapped onto the model (Fig. 1f and Supplementary Table 4). Six cross-links were identified between the transducer domain of TOP6BL and the 5Y-CAP domain of SPO11, reinforcing a stable interaction between SPO11 and TOP6BL (Fig. 1e). In addition, we observed 35 inter- and intramolecular cross-links within SPO11 molecules and 28 within TOP6BL molecules, supporting the potential formation of a heterotetramer in solution (Fig. 1f).

To test this, we first used co-immunoprecipitation assays. His–MBP–SPO11, TOP6BL–Flag and TOP6BL–tStrep (C-terminally Twin-Strep-tagged TOP6BL) proteins were co-expressed in Expi293F cells. Co-immunoprecipitation results showed that TOP6BL–Flag co-precipitates with both TOP6BL–tStrep and His–MBP–SPO11, indicating associations between TOP6BL proteins and between SPO11 and TOP6BL proteins (Fig. 1g). These associations suggest the formation of SPO11 and TOP6BL homodimers, as well as heterodimeric and potentially heterotetrameric SPO11–TOP6BL complexes within cells. To further validate the potential for heterotetramer formation, we performed pull-down experiments using complexes of His–SPO11–TOP6BL–Flag and His–MBP–SPO11–TOP6BL–tStrep purified from Expi293F cells (Fig. 1h and Extended Data Fig. 1b–d). The results show that TOP6BL–Flag can pull down TOP6BL–tStrep, His–SPO11 and His–MBP–SPO11 proteins (Fig. 1i), indicative of the formation of heterotetramers in solution. On the basis of these findings, we proposed that the heterotetramer formation might be inefficient in solution, whereas the heterodimer might form more readily and exhibit greater stability.

High-affinity binding of the complex to DNA ends

To investigate SPO11 binding affinity, we conducted electrophoretic mobility shift assays (EMSAs) with various oligonucleotides[21]. We designed five oligonucleotides with varied terminal structures (Supplementary Table 5): double 5′ overhang (two strands with 2-nt 5′ overhangs); single 5′ overhang (one strand with a 2-nt 5′ overhang); 3′ overhang (one strand with 2-nt 3′ overhang); blunt end (no overhangs); and double hairpin (nicked DNA) (Extended Data Fig. 3a). The results show that the single 5′ overhang has a dissociation constant (K_d) of 30.5 ± 2.63 nM, indicating a 1.5-fold weaker affinity compared with the double 5′ overhang (K_d of 20.8 ± 0.39 nM) (Extended Data Fig. 3a,b). The 3′ overhang and blunt end show similar affinities, with K_d values of 43.5 ± 2.15 nM and 47.8 ± 2.14 nM, respectively, both approximately twofold weaker than that of the double 5′ overhang structure (Extended Data Fig. 3a,b). In addition, the double hairpin has a binding affinity of 68.4 ± 3.06 nM, which is weaker than that of both the double 5′ overhang and the single 5′ overhang (Extended Data Fig. 3a,b). These findings suggest that SPO11 binds more efficiently to structures with 5′ overhangs, which is consistent with the binding patterns observed for yeast Spo11 (ref. 21).

Reconstitution of meiotic DSB formation in vitro

We assessed the catalytic activity of mammalian SPO11 by evaluating its ability to cleave plasmid-based substrates mimicking DSB formation. Both His–SPO11 and its MBP fusion variant efficiently cleaved the substrates (Fig. 2a,b and Extended Data Fig. 4a,c). Time-course experiments showed that both the His–SPO11–TOP6BL–Flag complex and the His–MBP–SPO11–TOP6BL–Flag complex progressively convert supercoiled DNA (scDNA) into linear plasmids, with the reaction plateauing after one hour (Fig. 2a,b and Extended Data Fig. 4a,c). The gradual disappearance of scDNA bands, along with the rising linear and nicked DNA bands, indicates successful scDNA cleavage by His–MBP–SPO11. (Fig. 2a,b). For simplicity, the His–MBP–SPO11–TOP6BL–Flag complex is referred to as SPO11–TOP6BL hereafter. Notably, a faint smear was observed below the linear DNA at the final time point in reactions with the SPO11–TOP6BL complex (Fig. 2a), suggesting the possibility of further cleavage by the complex. To test this, we used linear plasmid DNA as a substrate and found that it was cleaved by the SPO11–TOP6BL complex as well (Extended Data Fig. 4d,e). These results underscore the efficient DNA-cleavage capability of the mouse SPO11–TOP6BL complex in vitro.

SPO11 initiates DSB formation through a topoisomerase-like mechanism to establish a covalent bond with DNA[1,2,26]. This covalent attachment occurs at the DSB end through a nucleophilic attack by a tyrosine residue on the phosphodiester bond of the DNA[1,2,26]. Structural alignment of the predicted SPO11 structure with the crystal structure of African swine fever virus (Asfv) topoisomerase II in complex with gate-DNA (G-DNA) and transport-DNA (T-DNA) (Protein Data Bank ID: 8XRI) highlighted Y138 as crucial for interacting with the DNA backbone, consistent with the key role of Y138 in mouse meiosis in vivo[27–29] (Fig. 2c). We purified mutant SPO11–TOP6BL complexes, specifically Y137F, Y138F and the double mutant Y137F/Y138F (Fig. 2d and Extended Data Fig. 1c). Cleavage assays revealed that both the Y138F and the Y137F/Y138F mutations completely abolish activity, highlighting the indispensable role of Y138 (Fig. 2e,f). By contrast, despite the high conservation of Y137 (except for in yeast, some plants and certain protists, in which there is a phenylalanine residue before the catalytic tyrosine[17,30]; Supplementary Fig. 1), the Y137F mutant retains activity nearly equivalent to that of the wild type (Fig. 2e,f). Time-course experiments further confirmed the complete loss of activity in the Y138F mutant, which showed no activity even after two hours, whereas Y137F maintained activity comparable to that of the wild type (Fig. 2e,f and Extended Data Fig. 4b,c). However, we observed that a high molar excess of the protein complex relative to DNA was required for cleavage in these reactions. To investigate this requirement, we conducted DNA titrations at a constant concentration of the protein complex. We found that increasing the plasmid DNA concentration resulted in reduced cleavage efficiency (Fig. 2g,h). We then titrated the protein complex in reactions with either low or high concentrations of plasmid DNA. In reactions with lower DNA concentrations, the overall level of cleavage was higher, compared with those with higher DNA concentrations; nevertheless, in both conditions, cleavage increased as the protein levels increased (Extended Data Fig. 4f,g). These findings suggest that the ratio of protein complex to DNA is a limiting factor for the cleavage reaction.

To ascertain whether SPO11 forms a covalent bond with the end of its cleaved DNA strands, we analysed dead-end complexes of DNA and SPO11. Initial assays showed that protein–DNA conjugates, indicated by smear bands on the gel after 1% SDS treatment, were eliminated by treatment with proteinase K, confirming the presence of covalent bonds (Fig. 3a). The Y137F mutant behaved similarly to the wild type, whereas the Y138F mutant did not form the smear band, suggesting

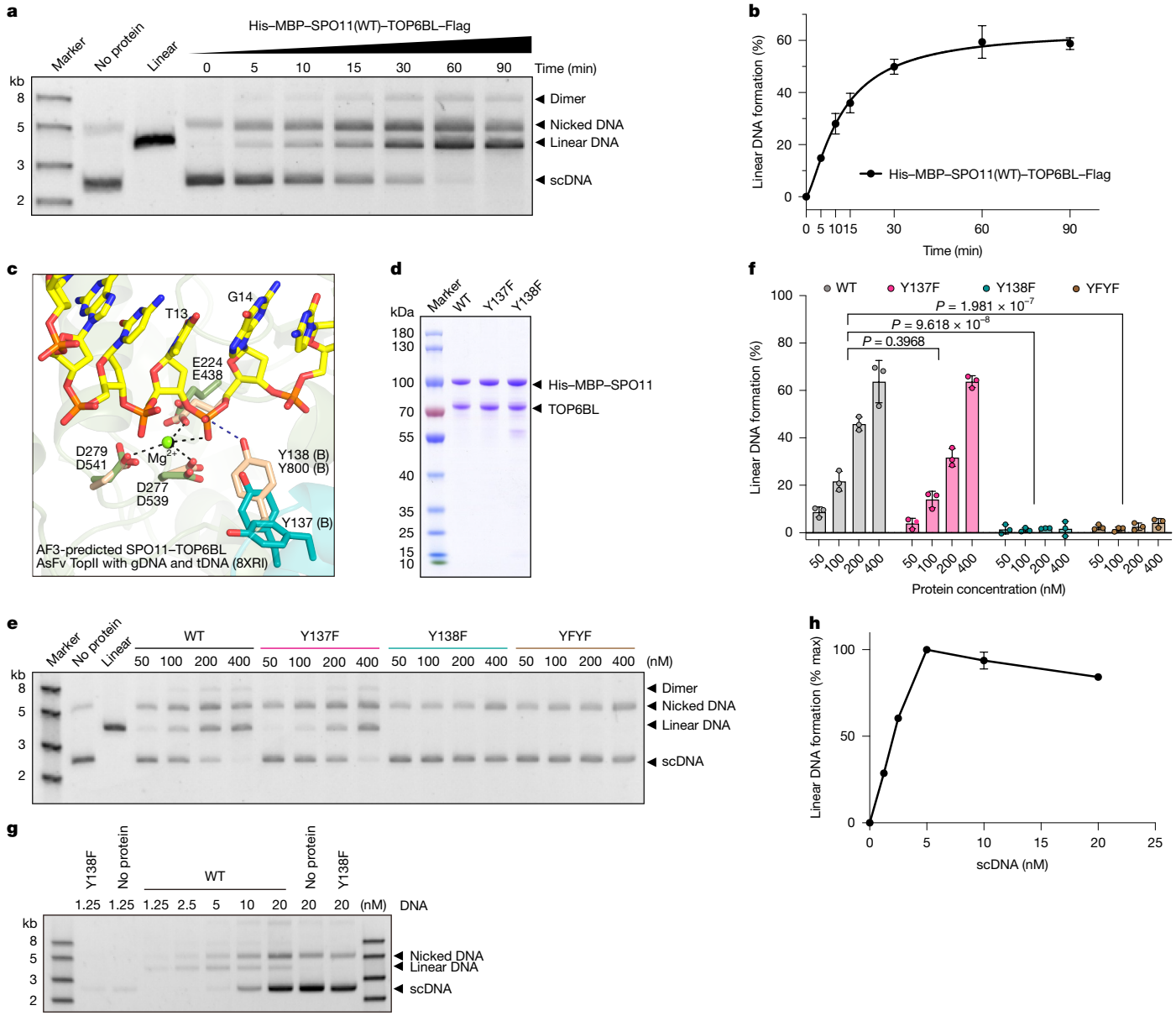

Fig. 2 | Characterization of SPO11–TOP6BL DNA-cleavage activity. a, Time course of the cleavage assay performed on plasmid DNA using the His–MBP–SPO11–TOP6BL–Flag complex at a concentration of 400 nM, observed at various time points. WT, wild type. **b**, Graphical representation of the kinetics of linear DNA formation from **a** over time ($n = 3$ independent experiments; mean ± s.d.). **c**, Structural alignment of the catalytic centre of the AlphaFold 3 (AF3)-predicted SPO11–TOP6BL complex with that of the AsFv Top2 in complex with gDNA and tDNA (Protein Data Bank ID: 8XRI). This comparison highlights the conserved features pertinent to catalytic function. **d**, SDS–PAGE analysis showing the purity of purified His–MBP–SPO11–TOP6BL–Flag wild type and its Y137F and Y138F mutants ($n = 3$ independent experiments). **e**, Cleavage activity assay comparing wild-type His–MBP–SPO11–TOP6BL–Flag with Y137F, Y138F and Y137F/Y138F (YFYF) mutants at protein concentrations of 50, 100, 200 and 400 nM. **f**, Quantification of relative cleavage activities from **e** ($n = 3$ independent experiments; mean ± s.d., adjusted P values are shown). **g**, DNA titration assay showing the cleavage activity of His–MBP–SPO11–TOP6BL–Flag with varying concentrations of plasmid DNA, with Y138F serving as a negative control. The assay was performed with 400 nM His–MBP–SPO11–TOP6BL–Flag while titrating plasmid DNA concentrations ($n = 3$ independent experiments). **h**, Quantifications show the mean and range from three independent experiments. Because the plasmid DNA concentrations were not constant, the greyscale values were normalized by dividing by the highest cleavage signal observed in each experiment ($n = 3$ independent experiments; mean ± s.d.).

that SPO11—not TOP6BL—is responsible for the covalent attachment (Fig. 3a). We then performed immunoprecipitation experiments with His–MBP-tagged SPO11 to further test whether SPO11 binds to cleavage DNA molecules. As expected, the cleaved linear DNA was recovered in the anti-His precipitate from reactions involving the SPO11–TOP6BL complex. By contrast, the Y138F-mutant complex did not yield any cleaved DNA (Fig. 3b).

To determine whether SPO11 binds to the 5′ terminus of its cleaved DNA strands, we took two approaches. First, we purified human tyrosyl-DNA phosphodiesterase 2 (TDP2) protein, known for resolving covalent adducts from DNA by specifically hydrolysing the 5′-phosphodiester bond at the 5′ terminus of DSBs in DNA, thereby yielding DNA molecules with a free 5′ phosphate[31–33]. After an 0.5-h incubation with human TDP2, the band representing the SPO11–DNA adduct disappeared, indicating the 5′-phosphodiesterase activity in creating a 'clean' DSB suitable for recombination at the 5′ terminus of DSBs (Fig. 3c). Second, we synthesized two 46-bp fluorescently labelled DNA substrates for cleavage assays, with Cy3 labels on either the 5′ or

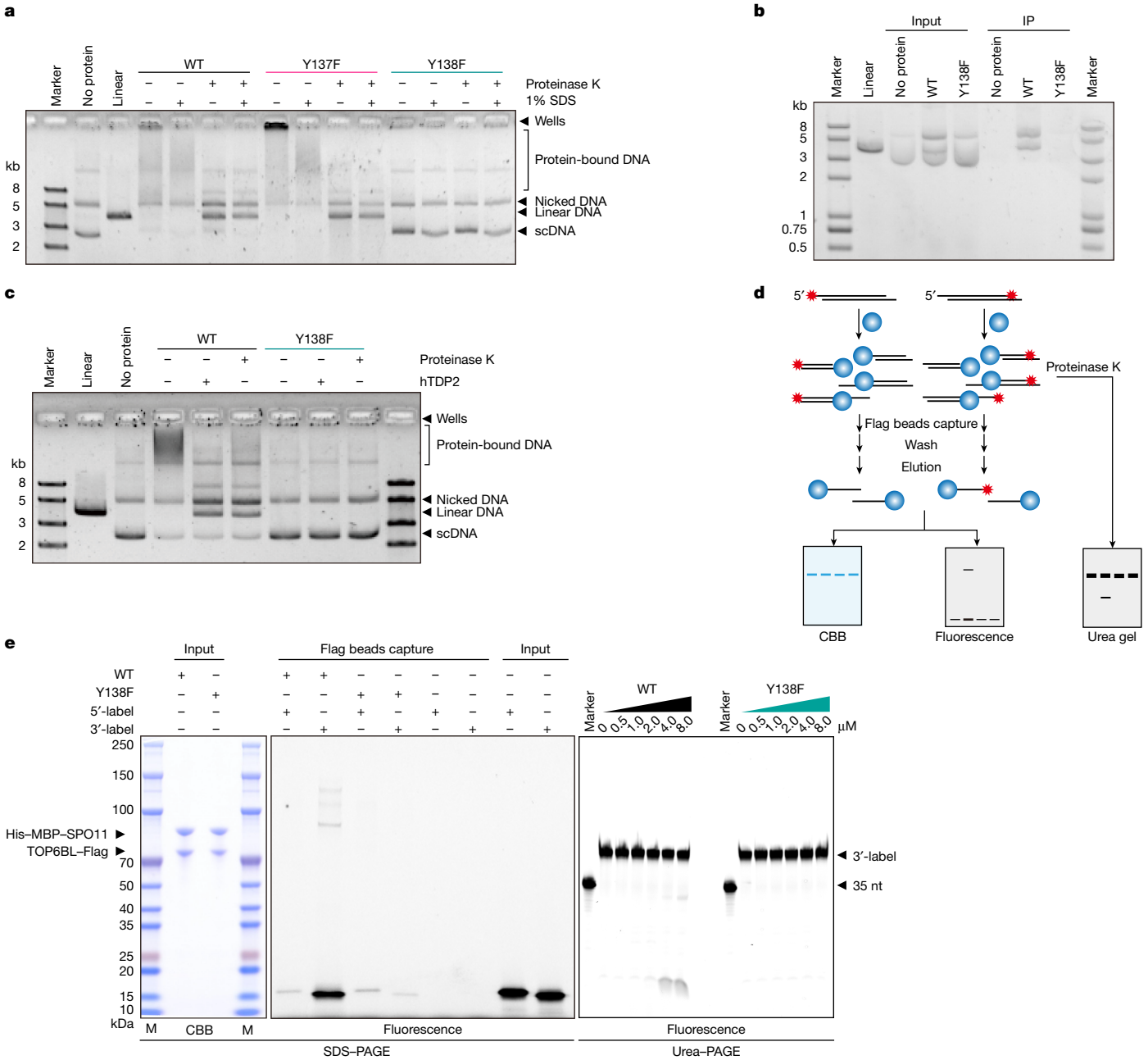

Fig. 3 | Covalent binding and DNA-binding affinity of the SPO11–TOP6BL complex. a, Covalent-binding products of wild-type SPO11 and Y137F and Y138F mutant SPO11 complexes with TOP6BL and cleaved DNA were assessed after treatment with either proteinase K or SDS. In the absence of proteinase K treatment, the reaction products from wild-type and Y137F SPO11 exhibited diffuse bands, indicative of covalent linkage between SPO11 and DNA ($n = 3$ independent experiments). **b**, Immunoprecipitation (IP) assay detecting SPO11–DNA conjugates. Wild-type and Y138F mutant complexes were reacted with plasmid DNA, immunoprecipitated using anti-His antibodies, treated with proteinase K and analysed on agarose gels to detect DNA bands indicative of cleavage ($n = 3$ independent experiments). **c**, Reaction products from SPO11–TOP6BL-mediated plasmid cleavage were exposed to different temperatures, treated with human TDP2 (hTDP2) to cleave protein–5′-DNA linkages and analysed using agarose gel electrophoresis. The diffuse band disappeared after the denaturation of protein at 70 °C and subsequent treatment with human TDP2 ($n = 3$ independent experiments). **d**, Schematic diagram of cleavage assay and SDS–PAGE analysis of covalent SPO11–DNA complexes using wild-type or mutant SPO11 with 3′ or 5′ fluorescently labelled oligo. **e**, Validation of SPO11 forming a covalent bond with the 5′ end after cleavage. SDS–PAGE confirmed the presence of wild-type and Y138F-mutant proteins, and fluorescence scanning showed DNA signals at the SPO11 position only when the 3′ end of the 46-bp oligonucleotide substrate was labelled with Cy3. This indicates that SPO11 covalently attaches to the 5′ end after cleavage. In addition, urea–PAGE was used to detect the cleaved DNA fragments. Two main fragments observed on the urea gel suggest a preferred cleavage site within the 46-bp oligonucleotide ($n = 3$ independent experiments).

the 3′ end of the sense strand (Fig. 3d and Supplementary Table 5). A fluorescent signal, corresponding to the size of His–MBP–SPO11, was detected in reactions with the 3′-Cy3-labelled substrate, whereas no fluorescent band was observed with the 5′-Cy3-labelled substrate, revealing that SPO11 binds specifically to the 5′ end of the DNA strand (Fig. 3e). The Y138F mutant did not cleave either the 5′-labelled or the 3′-labelled substrate, and no fluorescent signal was observed (Fig. 3e). These findings reveal that SPO11 specifically forms a covalent attachment to the 5′ terminus of DSBs after cleaving DNA in vitro, mimicking the in vivo process of DSB formation.

In summary, we have successfully reconstituted meiotic DSB formation triggered by SPO11–TOP6BL in vitro.

Substrate preferences at cleavage sites

To investigate whether the SPO11–TOP6BL complex exhibits DNA sequence specificity for its cleavage, we mapped cleavage sites using END-seq[34]. In this method, DSB positions are mapped by blunting single-stranded DNA overhangs with the nucleases ExoVII and ExoT, ligating sequencing adaptors to the blunted ends and sequencing the ssDNA–DSB junctions[34] (Extended Data Fig. 5a). Using pEBZSH plasmid DNA as a substrate, we identified 30 reproducible break sites, each with at least 1.6 enrichment in the presence of the SPO11–TOP6BL complex compared with controls treated with the Y138F-mutant complex (Extended Data Fig. 5b–e). Pearson's correlation analysis showed that there was a high degree of reproducibility between two biological replicates (Extended Data Fig. 5b). Visual inspection revealed a thymine nucleotide preference at position +1 (87%, 26 out of 30) and a subtle guanine nucleotide at position −3 (43%, 13 out of 30), relative to the dyad axis cleavage sites in pEBZSH (Extended Data Fig. 5c–e), suggesting a mild sequence bias at SPO11 complex cleavage sites.

SPO11 cleavage activity requires Mg^{2+} but not ATP

Structural analysis with the AsFv Top2 structure suggested that residues E224, D277 and D279 in SPO11 might serve as coordination sites for Mg^{2+} ions (Fig. 2c). In the AsFv Top2 structure, Mg^{2+} further coordinates with the scissile phosphate[29]. To investigate the ion selectivity and catalytic potential of SPO11, we tested various divalent ions. SPO11 exhibited catalytic activity in the presence of Mg^{2+} and Mn^{2+} but showed negligible activity with Ca^{2+} (Fig. 4a,b). Notably, Mn^{2+} supports substantially stronger cleavage activity than Mg^{2+} (Fig. 4a,b). The enzyme activity was enhanced at lower Mg^{2+} concentrations and decreased at higher concentrations, underscoring the nuanced regulatory role of Mg^{2+} in SPO11 function (Fig. 4a,b).

Concurrently, we assessed the effect of nucleoside triphosphates (NTPs) on enzyme activity and found that the SPO11 catalytic activity does not require ATP. At 0.1 mM ATP, there was no significant alteration in activity (Fig. 4c,d). However, increasing the ATP concentration led to decreased activity, possibly because ATP occupies Mg^{2+} coordination sites and competes for the SPO11 DNA-binding site (Fig. 4c,d). The effects of other nucleotides, including GTP, CTP, UTP and the four dNTPs (deoxy-ribonucleoside triphosphates), were consistent with those of ATP, further indicating that the enzymatic activity of SPO11 is ATP-independent (Fig. 4c,d and Extended Data Fig. 6).

To confirm the importance of Mg^{2+} binding for the in vitro DSB-formation activity of SPO11, we constructed and purified three mutants: E224Q, D277N and D279N (Fig. 4e). All mutants exhibited substantially reduced plasmid-cleaving activity, with the D277N mutation showing the most pronounced effect (Fig. 4f,g). To further evaluate the biological importance of the Mg^{2+}-binding pocket in SPO11 in vivo, we generated a knock-in mouse model in which the Mg^{2+}-binding aspartate 277 residue is replaced by asparagine (*Spo11*^{D277N}, hereafter referred to as *Spo11*$^{DN/DN}$), using CRISPR–Cas9 targeting (Extended Data Fig. 7a). At 19 days postpartum (dpp), we observed that male germ cells in control (*Spo11*$^{DN/+}$) mice developed to the round spermatid stage. By contrast, the most advanced germ cells in *Spo11*$^{DN/DN}$ testes were zygotene-like spermatocytes, accompanied by an accumulation of apoptotic cells (Extended Data Fig. 7b). By 12 dpp, the ovarian cortex of wild-type mice contained numerous primordial follicles, whereas the cortex of *Spo11*$^{DN/DN}$ ovaries was nearly devoid of primordial follicles (Extended Data Fig. 7c,d). Chromosome spreading with immunostaining for antibodies against RPA2 (a marker for DSB repair), phospho-histone H2AX (γH2AX, a marker for the DNA damage response) and SYCP1 (a marker for synapsis) revealed that *Spo11*$^{DN/DN}$ spermatocytes lacked meiotic DSBs, resulting in defects in recombination and synapsis (Fig. 4h–j and Extended Data Fig. 8). These findings show that meiosis is arrested at early prophase I in *Spo11*$^{DN/DN}$ mice, similar to what is seen in *Spo11*$^{-/-}$ mice[11,12], confirming the essential role of the metal-binding residue in SPO11-catalysed DSBs.

Collectively, our results reveal that the DNA-cleavage activity of mouse SPO11–TOP6BL requires Mg^{2+} coordination through residues E224, D277 and D279 in SPO11, but does not depend on ATP—distinct from the ancestral topo VI enzyme.

Discussion

A central yet unresolved question in meiotic recombination is the biochemical characterization of the DSB-forming machinery. In this work, we successfully reconstitute the formation of meiotic DSBs in vitro, characterized by efficient DNA cleavage with the SPO11–TOP6BL complex and covalent attachment to the 5′ terminus of cleaved DNA, and reveal key divergences between the complex and its ancestral enzyme, topo VI.

We show that the DNA-cleavage activity of the mouse SPO11 complex is Mg^{2+}-dependent, exhibiting a catalytic mechanism akin to that of archaeal topo VI. This is further supported by our finding that mutation of the Mg^{2+}-binding residue (D277N) in SPO11 abolishes meiotic DSB formation in mice. However, unlike topo VI, which requires ATP for its activity, the mouse SPO11 complex does not depend on ATP for DNA cleavage. This distinction might reflect an evolutionary adaptation in SPO11 function specific to meiotic DSB formation. Indeed, mouse TOP6BL is proposed to contain degenerated ATP-binding and hydrolysis sites[19,20,35].

It is well-established that topo VI, which is an evolutionary precursor to the SPO11–TOP6BL complex, functions as an A_2B_2 heterotetramer comprising a dimer of heterodimers (VIA_2VIB_2). Although the mouse SPO11 and TOP6BL complex shows efficient DNA cleavage in vitro, we unexpectedly found that the mouse SPO11–TOP6BL complex efficiently forms a stable heterodimer with a 1:1 stoichiometry. Cross-linking experiments reveal potential tetrameric products; however, their proportion on SDS–PAGE was considerably lower than that of the cross-linked dimeric products (Fig. 1d). Moreover, pull-down and co-immunoprecipitation experiments support the presence of potential tetrameric complexes in solution. These findings suggest that the SPO11–TOP6BL complex undergoes tetramerization at higher protein concentrations but predominantly exists as a heterodimer at lower concentrations. This concentration-dependent tetramerization probably influences the efficiency of in vitro DNA cleavage, because higher protein concentrations promote tetramer formation, which is required for full catalytic activity.

Unlike archaeal topo VI, in which both topo VIa and topo VIb subunits can dimerize, AlphaFold 3 predictions suggest that the dimerization of mouse SPO11 alone or TOP6BL alone is unfavourable, as indicated by the PAE plot, the pTM (template modelling) scores, the ipTM (interface predicted template modelling) scores and conformational analyses (Extended Data Fig. 9a–d). Notably, AlphaFold 3 predictions reveal that the SPO11–TOP6BL complex bound to DNA forms a more stable structure, with improvements in the PAE plot and the pTM and ipTM scores (Extended Data Fig. 2b). This supports the idea that DNA binding promotes heterotetramerization of the SPO11–TOP6BL complex, consistent with the in vitro observation that, in the presence of a lower-DNA substrate, the SPO11–TOP6BL complex cleaved DNA efficiently even at a low protein concentration. This model also suggests that DNA binds in a bent confirmation within a groove formed by two SPO11 molecules (Extended Data Fig. 2a), potentially explaining the higher activity of the SPO11–TOP6BL complex on scDNA than on linear DNA.

In contrast to the ability of the SPO11–TOP6BL complex to cleave DNA alone in vitro, SPO11-catalysed DSB formation in vivo requires additional cofactors, such as REC114, MEI4 and IHO1. Previous studies[35]

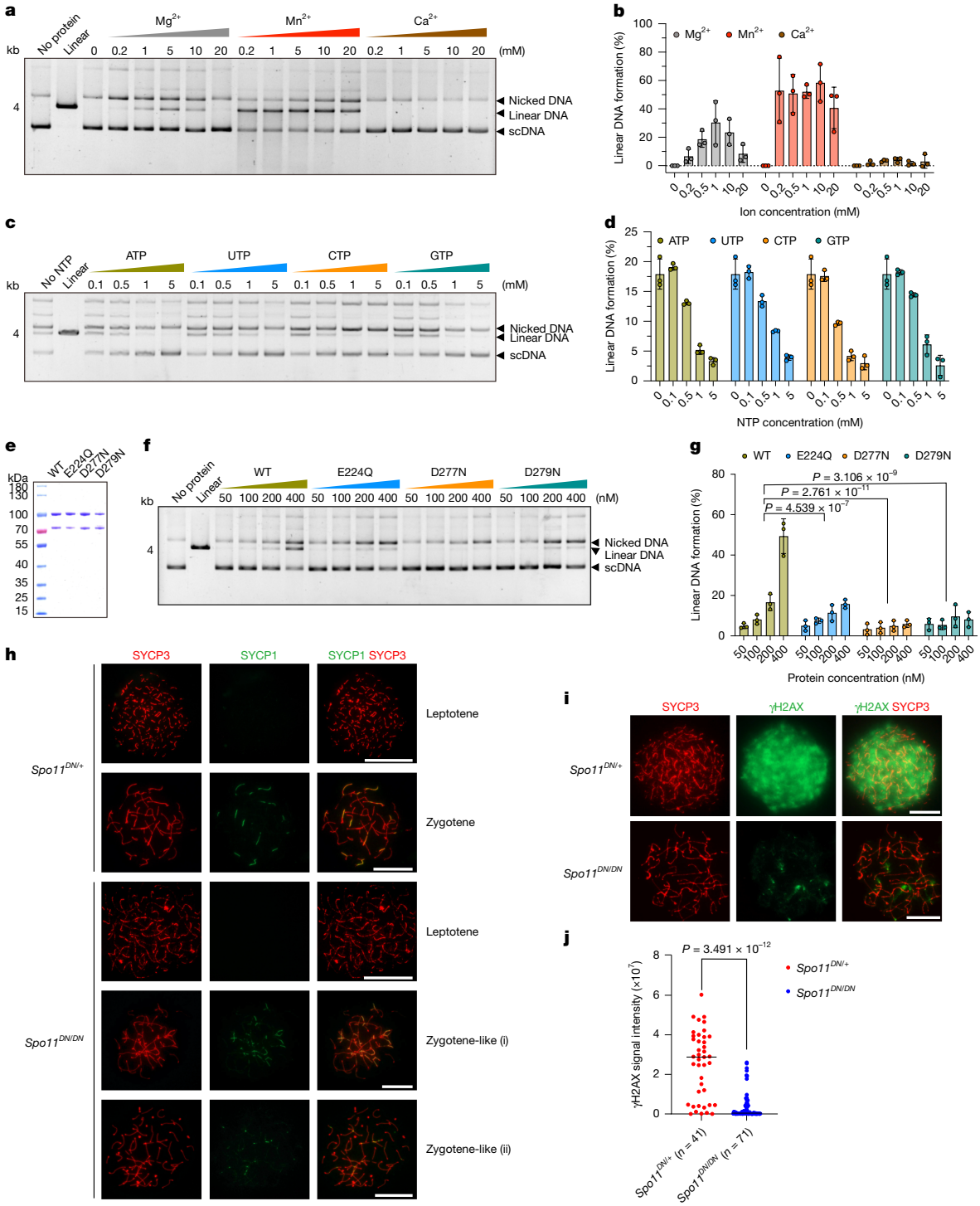

Fig. 4 | The cleavage activity of SPO11 depends on Mg^{2+} and is inhibited by NTPs. a, Analysis of the effects of divalent ions on the plasmid-cleaving activity of the MBP–SPO11–TOP6BL complex (at 200 nM). **b**, Quantitative effects of various divalent ions on cleavage activity, as illustrated in **a** ($n = 3$ independent experiments; mean ± s.d.). **c**, Effects of NTPs on the plasmid-cleaving activity of the MBP–SPO11–TOP6BL complex (at 400 nM). **d**, Statistical analysis of the effects of NTPs on cleavage activity, as presented in **c** ($n = 3$ independent experiments; mean ± s.d.). **e**, SDS–PAGE analysis showing the purity of wild-type MBP–SPO11 and various mutants, each in complex with TOP6BL ($n = 3$ independent experiments). **f**, Evaluation of the cleavage activity of wild-type MBP–SPO11 and various mutants, highlighting differences in catalytic performance. **g**, Quantitative effects of the various mutants on cleavage activity, as shown in **f** ($n = 3$ independent experiments; mean ± s.d., adjusted P values are shown). **h**, SYCP1 (green) and SYCP3 (red) were detected on chromosome spreads of spermatocytes from control ($Spo11^{DN/+}$) and $Spo11^{DN/DN}$ mutant spermatocytes. Defective synapsis in mutant spermatocytes is highlighted by co-staining of SYCP1 and SYCP3. In control mice, synapsis starts at zygotene, presenting as short fragments of synaptonemal complex (SC; yellow owing to overlapping SYCP1 and SYCP3 signals). In mutant mice, zygotene spermatocytes (named zygotene-like) have abnormal nuclei, characterized by (i) synapses between non-homologous chromosomes and (ii) short-synapsed SCs. Scale bars, 10 µm. **i**, SYCP3 (red) and γH2AX (green) were detected on chromosome spreads of spermatocytes from control and mutant spermatocytes. Scale bars, 10 µm. **j**, Quantification of total nuclear γH2AX signals on chromosome spreads of spermatocytes from control and mutant mice. n shows the numbers of cells analysed from four (control) and three (mutant) pooled experiments, respectively. P values were calculated by Mann–Whitney test (two-sided), with median γH2AX intensity marked. The original data of nuclear spreads can be found in the Supplementary Data.

have shown that the C-terminal α-helix of TOP6BL interacts with the Pleckstrin homology (PH) domain of REC114. Moreover, the yeast orthologues of REC114, MEI4 and IHO1 have been shown to assemble DNA-dependent condensates in vitro that recruit the yeast Spo11 core complex[36]. Thus, we speculate that in mice, the SPO11 complex can be recruited to the REC114–MEI4–IHO1 complex, resulting in the binding of REC114 to the C-terminal α-helix of TOP6BL. This interaction could promote the local concentration of the SPO11–TOP6BL complex, possibly together with DNA, thereby facilitating tetramer formation to enhance cleavage efficiency in vivo. Future studies will be needed to determine the structural details of the SPO11 and TOP6BL complex that induce meiotic DSB formation, and to elucidate the precise roles of its components in dimerization and function.

Online content

Any methods, additional references, Nature Portfolio reporting summaries, source data, extended data, supplementary information, acknowledgements, peer review information; details of author contributions and competing interests; and statements of data and code availability are available at https://doi.org/10.1038/s41586-024-08551-1.

1. Bergerat, A. et al. An atypical topoisomerase II from archaea with implications for meiotic recombination. *Nature* **386**, 414–417 (1997).
2. Keeney, S., Giroux, C. N. & Kleckner, N. Meiosis-specific DNA double-strand breaks are catalyzed by Spo11, a member of a widely conserved protein family. *Cell* **88**, 375–384 (1997).
3. Gray, S. & Cohen, P. E. Control of meiotic crossovers: from double-strand break formation to designation. *Annu. Rev. Genet.* **50**, 175–210 (2016).
4. Hunter, N. Meiotic recombination: the essence of heredity. *Cold Spring Harb. Perspect. Biol.* **7**, a016618 (2015).
5. Grelon, M. Meiotic recombination mechanisms. *C. R. Biol.* **339**, 247–251 (2016).
6. Zickler, D. & Kleckner, N. Recombination, pairing, and synapsis of homologs during meiosis. *Cold Spring Harb. Perspect. Biol.* **7**, a016626 (2015).
7. Parvanov, E. D., Petkov, P. M. & Paigen, K. *Prdm9* controls activation of mammalian recombination hotspots. *Science* **327**, 835 (2010).
8. Baudat, F. et al. PRDM9 is a major determinant of meiotic recombination hotspots in humans and mice. *Science* **327**, 836–840 (2010).
9. Baudat, F., Imai, Y. & de Massy, B. Meiotic recombination in mammals: localization and regulation. *Nat. Rev. Genet.* **14**, 794–806 (2013).
10. Lange, J. et al. The landscape of mouse meiotic double-strand break formation, processing, and repair. *Cell* **167**, 695–708 (2016).
11. Myers, S. et al. Drive against hotspot motifs in primates implicates the *PRDM9* gene in meiotic recombination. *Science* **327**, 876–879 (2010).
12. Baudat, F., Manova, K., Yuen, J. P., Jasin, M. & Keeney, S. Chromosome synapsis defects and sexually dimorphic meiotic progression in mice lacking Spo11. *Mol. Cell* **6**, 989–998 (2000).
13. Romanienko, P. J. & Camerini-Otero, R. D. The mouse *Spo11* gene is required for meiotic chromosome synapsis. *Mol. Cell* **6**, 975–987 (2000).
14. Graille, M. et al. Crystal structure of an intact type II DNA topoisomerase: insights into DNA transfer mechanisms. *Structure* **16**, 360–370 (2008).
15. Bergerat, A., Gadelle, D. & Forterre, P. Purification of a DNA topoisomerase II from the hyperthermophilic archaeon *Sulfolobus shibatae*. A thermostable enzyme with both bacterial and eucaryal features. *J. Biol. Chem.* **269**, 27663–27669 (1994).
16. Brinkmeier, J., Coelho, S., de Massy, B. & Bourbon, H. M. Evolution and diversity of the TopoVI and TopoVI-like subunits with extensive divergence of the TOPOVIBL subunit. *Mol. Biol. Evol.* **39**, msac227 (2022).
17. Malik, S. B., Ramesh, M. A., Hulstrand, A. M. & Logsdon, J. M. Jr. Protist homologs of the meiotic *Spo11* gene and topoisomerase VI reveal an evolutionary history of gene duplication and lineage-specific loss. *Mol. Biol. Evol.* **24**, 2827–2841 (2007).
18. Nichols, M. D., DeAngelis, K., Keck, J. L. & Berger, J. M. Structure and function of an archaeal topoisomerase VI subunit with homology to the meiotic recombination factor Spo11. *EMBO J.* **18**, 6177–6188 (1999).
19. Robert, T. et al. The TopoVIB-like protein family is required for meiotic DNA double-strand break formation. *Science* **351**, 943–949 (2016).
20. Vrielynck, N. et al. A DNA topoisomerase VI-like complex initiates meiotic recombination. *Science* **351**, 939–943 (2016).
21. Claeys Bouuaert, C. et al. Structural and functional characterization of the Spo11 core complex. *Nat. Struct. Mol. Biol.* **28**, 92–102 (2021).
22. Yu, Y. et al. Cryo-EM structures of the Spo11 core complex bound to DNA. *Nat. Struct. Mol. Biol.* https://doi.org/10.1038/s41594-024-01382-8 (2024).
23. Zheng, Z. et al. Reconstitution of SPO11-dependent double-strand break formation. *Nature* https://doi.org/10.1038/s41586-025-08601-2 (2025).
24. Oger, C. & Claeys Bouuaert, C. SPO11 dimers are sufficient to catalyse DNA double-strand breaks in vitro. *Nature* https://doi.org/10.1038/s41586-024-08574-8 (2025).
25. Corbett, K. D., Benedetti, P. & Berger, J. M. Holoenzyme assembly and ATP-mediated conformational dynamics of topoisomerase VI. *Nat. Struct. Mol. Biol.* **14**, 611–619 (2007).
26. Lam, I. & Keeney, S. Mechanism and regulation of meiotic recombination initiation. *Cold Spring Harb. Perspect. Biol.* **7**, a016634 (2014).
27. Carofiglio, F. et al. SPO11-independent DNA repair foci and their role in meiotic silencing. *PLoS Genet.* **9**, e1003538 (2013).
28. Boateng, K. A., Bellani, M. A., Gregoretti, I. V., Pratto, F. & Camerini-Otero, R. D. Homologous pairing preceding SPO11-mediated double-strand breaks in mice. *Dev. Cell* **24**, 196–205 (2013).
29. Yang, J. et al. Structures of African swine fever virus topoisomerase complex and their implications. *Nat. Commun.* **15**, 6484 (2024).
30. Hartung, F. et al. The catalytically active tyrosine residues of both SPO11-1 and SPO11-2 are required for meiotic double-strand break induction in *Arabidopsis*. *Plant Cell* **19**, 3090–3099 (2007).
31. Hornyak, P. et al. Mode of action of DNA-competitive small molecule inhibitors of tyrosyl DNA phosphodiesterase 2. *Biochem. J.* **473**, 1869–1879 (2016).
32. Schellenberg, M. J. et al. Reversal of DNA damage induced topoisomerase 2 DNA–protein crosslinks by Tdp2. *Nucleic Acids Res.* **44**, 3829–3844 (2016).
33. Gao, R. et al. Proteolytic degradation of topoisomerase II (Top2) enables the processing of Top2·DNA and Top2·RNA covalent complexes by tyrosyl-DNA-phosphodiesterase 2 (TDP2). *J. Biol. Chem.* **289**, 17960–17969 (2014).
34. Paiano, J. et al. ATM and PRDM9 regulate SPO11-bound recombination intermediates during meiosis. *Nat. Commun.* **11**, 857 (2020).
35. Nore, A. et al. TOPOVIBL–REC114 interaction regulates meiotic DNA double-strand breaks. *Nat. Commun.* **13**, 7048 (2022).
36. Claeys Bouuaert, C. et al. DNA-driven condensation assembles the meiotic DNA break machinery. *Nature* **592**, 144–149 (2021).

Methods

Generation of knock-in mice by CRISPR–Cas9 targeting

The *Spo11*^{D277N} mouse line was generated by Shanghai Biomodel Organism using CRISPR–Cas9 technology. The donor oligos were designed to change the D277 codon GAT (D) to AAT (N). The resulting point-mutation founders were back-crossed with C57BL/6J mice to obtain heterozygous mutant mice. The heterozygous mutants were crossbred to generate homozygous *Spo11*^{D277N} mutant mice. Genotyping of Spo11^{D277N} was done by PCR and DNA sequencing. The sequences of injected sgRNA, oligo donors and primers for genotyping are shown in Supplementary Table 1. Mice were fed regular rodent chow with ad libitum access to water and food in a 12-h light–dark cycle in a temperature and humidity-controlled environment (20–26 °C, 30–70% humidity). All animal experiments were performed according to the guidelines of the Animal Care and Use Committee at Shanghai Institute of Biochemistry and Cell Biology, Center for Excellence in Molecular Cell Science, Chinese Academy of Sciences. The experiments performed in this study were approved by the Ethics Committee of Center for Excellence in Molecular Cell Science, Chinese Academy of Sciences (2022-151).

Preparation of expression vectors

Expression vectors for N-terminally His–MBP-tagged SPO11 and C-terminally Flag-tagged TOP6BL were generated by cloning sequences derived from codon-optimized, synthesized mouse *Spo11* and *Top6bl* cDNA (Genewiz) into the pcDNA3.4-MBP vector and the pMC vector (a gift from J. Liu), respectively. To construct a version of TOP6BL with a C-terminal Twin-Strep tag (TOP6BL–tStrep), the *Top6bl* coding sequence was cloned into a pMC vector that had been modified to include the twin StrepII tag sequence at the 3′ end. To obtain SPO11 without the MBP tag, the pcDNA3.4-His-MBP-SPO11 construct was PCR-amplified using the SPO11_FO/RO primer pairs and self-ligated using MultiF Seamless Assembly Mix (ABclonal), according to the manufacturer's instructions. Point mutants were also generated using MultiF Seamless Assembly Mix (ABclonal). The sequences of the above-mentioned plasmid are shown in Supplementary Fig. 2. For plasmid coding for human TDP2, a DNA fragment encoding the full length of human TDP2 was cloned into the pET28-SMT3 vector between the BamHI and XhoI sites, which contains an N-terminal Ulp1-cleavable His_6–SUMO tag. The oligonucleotides for this study were synthesized by Sangon, and the plasmids used in this study are listed in Supplementary Tables 2 and 3.

Expression and purification of the mouse SPO11–TOP6BL complex

Three variants of mouse SPO11–TOP6BL complexes (His–SPO11–TOP6BL–Flag, His–MBP–SPO11–TOP6BL–Flag and His–SPO11–TOP6BL–tStrep) were expressed in Expi293F cells. For each complex, plasmids were co-transfected at a 1:1 mass ratio by 2 mg plasmids in 1 l culture. Cells were cultured in 4 l suspension at 37 °C with 5% CO_2 and 125 rpm orbital shaking. After 72 h, cells were collected (500*g*, 5 min) and lysed in buffer containing 25 mM HEPES, pH 7.5, 150 mM NaCl and 20 mM imidazole, 10% glycerol, 0.5% Triton X-100, 1 mM DTT and 1× protease inhibitor cocktail (Sparkjade) using a high-pressure crusher (Union, 300–500 Pa, 5 min). The lysate was clarified by centrifugation (48,000*g*, 90 min).

All three complexes were initially purified using nickel affinity chromatography. The supernatant was incubated with 2 ml pre-equilibrated Ni-NTA resin (QIAGEN) for 2 h. After washing with 200 ml buffer (25 mM HEPES, pH 7.5, 150 mM NaCl, 40 mM imidazole and 10% glycerol), proteins were eluted with 50 ml buffer containing 25 mM HEPES, pH 7.5, 150 mM NaCl, 300 mM imidazole, 10% glycerol, 1 mM DTT and 1× protease inhibitor cocktail.

Then, the eluate was supplemented with 10 mM EDTA and incubated with 1 ml pre-equilibrated Flag resin (Selleckchem) for 2 h. After washing with 50 ml buffer (50 mM Tris, pH 7.5, 150 mM NaCl, 10% glycerol), proteins were eluted with 5 ml buffer containing 50 mM Tris, pH 7.5, 150 mM NaCl, 10% glycerol, 0.1 mg ml^{-1} 3× Flag peptide (MCE), 1 mM DTT and 1× protease inhibitor cocktail.

For tStrep-tagged complex, the Ni-NTA eluate was incubated with 1 ml pre-equilibrated StrepTactin XT resin (IBA) for 2 h. After washing with 50 ml buffer (50 mM Tris, pH 7.5, 150 mM NaCl, 10% glycerol), proteins were eluted with 5 ml buffer containing 50 mM Tris, pH 7.5, 150 mM NaCl, 10% glycerol, 2.5 mM desthiobiotin, 1 mM DTT and 1× protease inhibitor cocktail.

All purified complexes were further fractionated by SEC using a Superdex 200 Increase 10/300 GL column (Cytiva) equilibrated in 20 mM HEPES, pH 7.5, 100 mM NaCl and 0.25 mM TCEP. The column was calibrated using Bio-Rad's Gel Filtration Standard (1511901). Protein concentrations were determined by Bradford assay (Thermo Fisher Scientific).

Co-immunoprecipitation

Expi293F cells were cultured in suspension and split into two 100-ml cultures. When the cell density reached approximately 3×10^6 cells per ml, one culture was transfected with plasmids encoding His–MBP–SPO11 (0.2 mg), TOP6BL–Flag (0.1 mg) and TOP6BL–tStrep (0.1 mg). The second culture was transfected with plasmids encoding His–MBP–SPO11 (0.1 mg) and TOP6BL–tStrep (0.1 mg). After 72 h, cells were collected by centrifugation at 500*g* for 5 min at 4 °C and resuspended in 25 ml lysis buffer containing 20 mM HEPES, pH 7.5, 100 mM NaCl, 0.25 mM Tris(2-carboxyethyl)phosphine (TCEP) and 1× protease inhibitor cocktail. Cells were lysed by gentle sonication on ice for 1 h. The lysates were clarified by centrifugation at 48,000*g* for 90 min at 4 °C.

For each sample, 10 ml of supernatant was incubated overnight at 4 °C with 50 µl of pre-equilibrated anti-Flag M2 affinity gel beads. After incubation, the beads were collected by centrifugation at 500*g* for 5 min at 4 °C and washed three times with 2 ml of wash buffer (20 mM HEPES, pH 7.5, 100 mM NaCl, 0.25 mM TCEP, 0.1% NP-40 and 1× protease inhibitor cocktail). Bound proteins were eluted by incubating the beads with 100 µl of elution buffer containing 20 mM HEPES, pH 7.5, 100 mM NaCl, 0.25 mM TCEP and 0.1 mg ml^{-1} Flag peptide for 1 h at 4 °C with gentle agitation.

Eluates were mixed with SDS–PAGE loading buffer, boiled at 95 °C for 5 min and analysed by western blotting using standard protocols. The tStrep tag was detected with StrepII tag mouse monoclonal antibody (HRP conjugated, AF2927, Beyotime), the Flag tag was detected with Flag tag mouse monoclonal antibody (HRP conjugated, AF2855-50µl, Beyotime) and the MBP tag was detected with MBP tag mouse monoclonal antibody (HRP conjugated, AF2915, Beyotime).

Pull-down assay

Fifty microlitres of anti-Flag M2 affinity gel beads were equilibrated with a binding buffer containing 20 mM HEPES, pH 7.5, 100 mM NaCl and 0.25 mM TCEP. In a total volume of 200 µl of binding buffer, 5 µg of purified His–MBP–SPO11–TOP6BL–Flag was mixed with varying amounts of His–SPO11–TOP6BL–Strep (0, 10, 25 or 50 µg) and added to the equilibrated Flag beads for incubation at 4 °C for 3 h with gentle rotation. After centrifugation at 500*g* for 5 min at 4 °C, the supernatant was removed, and the beads were washed three times with 1 ml binding buffer to eliminate unbound proteins. The beads were then resuspended in 50 µl elution buffer (20 mM HEPES, pH 7.5, 100 mM NaCl, 0.25 mM TCEP and 0.1 mg ml^{-1} Flag peptide) and incubated at 4 °C for 2 h with gentle agitation to elute bound proteins. The eluted proteins were analysed by western blotting, detecting the His tag with His tag mouse monoclonal antibody (HRP conjugated, AF2879-50µl, Beyotime). The remaining antibodies used for detecting the MBP, Flag and tStrep tags were the same as those used in the co-immunoprecipitation experiments.

Expression and purification of human TDP2

To express recombinant proteins, the plasmid containing the cDNA of full-length human *TDP2* was transformed into *Escherichia coli* BL21(DE3).

Cells were cultured in LB medium at 37 °C with 50 mg ml^{-1} kanamycin until the optical density at 600 nm reached 0.6–0.8. The cells were cooled at 18 °C for one hour before induction with 0.2 mM IPTG for 16 h. Cells were collected by centrifugation at 5,000 rpm for 10 min. Cell pellets were resuspended in lysis buffer containing 20 mM Tris, pH 8.0, 500 mM NaCl and 25 mM imidazole and lysed using a high-pressure homogenizer (Litu, FB-110×15). The cell lysates were centrifuged at 16,000 rpm for 1 h at 4 °C. The supernatants were then purified using a nickel-chelating affinity column (HisTrap, Cytiva), washed with lysis buffer and eluted with a buffer containing 20 mM Tris, pH 8.0, 500 mM NaCl and 500 mM imidazole. The target fusion protein was incubated with Ulp1 protease to remove the SUMO tag. The mixture was diluted fivefold with 20 mM Tris, pH 8.0 and loaded onto a HiTrap Q HP column (Cytiva) to remove the SUMO tag and Ulp1 protease. The eluate was concentrated onto a HiLoad 16/60 Superdex 200 column (Cytiva) equilibrated with a buffer containing 20 mM HEPES, pH 7.5 and 300 mM NaCl. The purified proteins were then concentrated and stored at −80 °C for subsequent use.

DNA-cleavage assays

For plasmid DNA-cleavage assays, a 4,000-bp T-vector (pEASY-Blunt, Trans) containing a SPO11 hotspot sequence (GRCm38p2/mm10 chr. 19: 59349669–59349759) was used as the substrate (hereafter referred to as pEBZSH)[21]. The reactions were conducted in 10 µl cleavage buffer containing 50 mM HEPES, pH 7.5, 30 mM KCl, 2 mM DTT and 1 mM $MgCl_2$, unless otherwise specified. Protein complexes and the plasmid substrate were initially prepared on ice.

Time-course experiments were performed to assess the kinetics of cleavage, using 400 nM concentrations of His–SPO11–TOP6BL–Flag, His–MBP–SPO11–TOP6BL–Flag and His–MBP–SPO11(Y138F)–TOP6BL–Flag. Each reaction contained 5 nM plasmid substrate and was incubated at 37 °C, with samples collected at intervals of 0, 5, 10, 15, 30, 60 and 90 min.

For mutational analysis, the catalytic activities of wild-type SPO11 and the mutants Y137F, Y138F and Y137F/Y138F were compared across protein concentrations of 50, 100, 200 and 400 nM. Metal-binding site mutants (E224Q, D277N and D279N) were analysed under the same concentration conditions.

To investigate metal-ion dependence, reactions included varying the concentrations of $MgCl_2$, $MnCl_2$ or $CaCl_2$, ranging from 0 to 20 mM. Nucleotide requirements were tested by supplementing with 0 to 5 mM ATP or other NTPs or dNTPs, with a constant protein concentration of 400 nM.

Substrate and protein titration experiments were designed to investigate the concentration effects. The effect of substrate concentration was evaluated at a constant protein concentration of 400 nM, with plasmid levels set between 1.25 and 20 nM. Conversely, protein concentration effects were assessed at fixed plasmid concentrations (1.25 nM and 20 nM), with protein titrated from 0 nM to 400 nM.

For linear DNA substrate preparation, the plasmid was digested by EcoRI (NEB) and purified with the FastPure Gel DNA extraction kit (Vazyme). Cleavage assays were performed with 400 nM of wild-type protein under two conditions: one adhering to standard buffer conditions, and the other substituting Mn^{2+} for Mg^{2+} while omitting KCl.

Reactions were terminated by adding 1 µl 10% SDS, 0.5 µl 500 mM EDTA and 0.8 µl proteinase K (Roche, 20 mg ml^{-1}), followed by incubation at 55 °C for 30 min. Reaction products were analysed by electrophoresis on 1% agarose gels in TAE buffer at 80 V for 60 min. Gels were stained with GelRed (Yeasen) and visualized using a Tanon 2500 imaging system. For each plasmid cleavage assay, an equal amount of linear DNA was included as a positive control. The production of linear DNA was quantified using ImageJ software.

Identification of the 5′ tyrosine–phosphate bond in SPO11–DNA

The SPO11 cleavage reactions were performed as described previously for the DNA-cleavage assays, using 400 nM His–MBP–SPO11–TOP6BL–Flag complex incubated with plasmid DNA at 37 °C for 30 min. The cleavage buffer consisted of 50 mM HEPES, pH 7.5, 30 mM KCl, 2 mM DTT and 1 mM $MgCl_2$.

To assess the formation of protein–DNA conjugates, reactions containing wild-type, Y137F or Y138F His–MBP–SPO11–TOP6BL–Flag complexes were processed with or without 1% SDS and proteinase K (Roche, 20 mg ml^{-1}). The samples were then loaded onto 1% agarose gels and subjected to electrophoresis in TAE buffer. After electrophoresis, the gels were stained with GelRed (Yeasen) for visualizing DNA bands.

For the immunoprecipitation assay, wild-type and Y138F complexes were reacted with plasmid DNA (total 500 µl). After the reaction, product was supplemented with 50 mM HEPES 7.5, 4 M urea and 250 mM NaCl, and then incubated with 25 µl pre-equilibrated Ni-NTA resin (QIAGEN). The beads were washed three times with 1 ml wash buffer (50 mM HEPES 7.5, 4 M urea and 250 mM NaCl). Bound complexes were eluted by incubating the beads with 25 µl elution buffer containing 1% SDS in 25 mM HEPES, pH 7.5, 150 mM NaCl and 10% glycerol for 10 min at room temperature with gentle mixing. The isolated complexes were treated with proteinase K, followed by analysis on agarose gels to check for the presence of DNA bands indicative of cleavage.

To examine the role of human TDP2 in cleaving the 5′ tyrosine–phosphate bond, wild-type and Y138F complexes were reacted with plasmid DNA. Reactions were terminated with a brief heating at 70 °C for 10 min to denature the SPO11–TOP6BL complex. Human TDP2 (800 nM) was added to the reactions, which were subsequently incubated at 37 °C for 30 min. Reactions were terminated with 1 µl of 10% SDS and 0.5 µl of 500 mM EDTA. The reaction products, with or without proteinase K and human TDP2 treatment, were analysed on agarose gels.

A 46-bp oligonucleotide substrate labelled with Cy3 fluorescence at either the 5′ or 3′ end was used to evaluate covalent-bond formation with SPO11. The sequence is SPO11 hotspot (GRCm38p2/mm10 chr. 6: 93618016-93618061)[21]. Reaction mixtures (10 µl total volume) contained 0.5 µM Cy3-labelled oligonucleotide and 2 µM of either wild-type or Y138F-mutant His–MBP–SPO11–TOP6BL–Flag complexes. The reactions were performed in buffer comprising 20 mM HEPES, pH 7.5, 30 mM KCl, 2 mM $MgCl_2$, 2 mM $MnCl_2$ and 5% (v/v) glycerol. After the cleavage reaction, Flag-tagged proteins and associated oligonucleotides were captured using anti-Flag affinity beads. The reaction mixtures were incubated with pre-equilibrated anti-Flag beads (50 µl) at 4 °C with gentle agitation for one hour in wash buffer containing 20 mM HEPES, pH 7.5, 100 mM NaCl, 0.1% NP-40, 0.25 mM TCEP and 1 mM EDTA. After binding, the beads were washed three times with the wash buffer to remove non-specifically bound materials. Each wash involved gently resuspending the beads for 15 min at 4 °C, followed by centrifugation at 500*g* for 2 min. Bound complexes were eluted by incubating the beads with 20 µl elution buffer containing 0.1 mg ml^{-1} Flag peptide in 20 mM HEPES, pH 7.5, 100 mM NaCl and 0.25 mM TCEP for 30 min at 4 °C with gentle mixing. Eluted products were analysed by SDS–PAGE, and fluorescence was detected using a Typhoon FLA 9000 gel imaging system (Cytiva) capable of detecting Cy3 fluorescence. For further analysis of reaction products, further reactions were performed at varying concentrations of His–MBP–SPO11–TOP6BL–Flag complexes. Reactions were terminated by adding SDS to a final concentration of 1% and EDTA to 50 mM (pH 8.0). Each sample was treated with 100 µg of proteinase K. All samples were subjected to 8 M urea–PAGE to separate cleavage fragments. The oligonucleotides (GenScript) used in this study are listed in Supplementary Table 5.

EMSA

The sequence of the PRDM9 hotspot motif was used for this study[21]. Purified His–MBP–SPO11–TOP6BL–Flag was incubated with Cy3-labelled DNA oligos at a final concentration of 10 nM in a binding buffer containing 20 mM HEPES, pH 7.5 and 30 mM KCl for 30 min at 4 °C. After incubation, bound and free DNA probes were separated by

6% native PAGE conducted at 4 °C. Cy3 fluorescence was visualized using a Typhoon FLA 9000 gel imaging system. The DNA-binding ratios were quantified by measuring the reduction in free DNA, with the grey value of free DNA quantified using ImageJ software. Oligonucleotides (GenScript) used in this study are listed in Supplementary Table 5.

XL-MS

The purified His–SPO11–TOP6BL–Flag complex was incubated with 0.25 mM, 0.5 mM or 1 mM DSS (Pierce, A39267) in a reaction buffer comprising 20 mM HEPES, pH 7.5 and 30 mM KCl at 25 °C for 30 min. The reaction was terminated by adding quenching buffer (50 mM Tris, pH 8.0) to a final concentration of 20 mM, followed by a 20-min incubation at room temperature. One-third of the sample was analysed using 10% SDS–PAGE and Coomassie blue staining to assess cross-linking efficiency. The remaining sample was precipitated with acetone. The protein pellet was dried using a Speedvac for 1–2 min. The pellet was subsequently dissolved in 8 M urea, 100 mM Tris, pH 8.5 and 5 mM TCEP (Thermo Fisher Scientific), and 10 mM iodoacetamide (Sigma) for reduction and alkylation was added to the solution, followed by incubation at room temperature for 30 min, respectively. The protein mixture was diluted four times and digested overnight with trypsin at 1:50 (w/w) (Promega). The digested peptide solutions were desalted using a MonoSpin C18 column (GL Science) and dried with a SpeedVac.

The peptide mixture was analysed by a homemade 30 cm-long pulled-tip analytical column (75 μm ID packed with ReproSil-Pur C18-AQ 1.9 μm resin, Dr. Maisch). The column was then placed in-line with an Easy-nLC 1200 nano HPLC (Thermo Fisher Scientific) for mass-spectrometry analysis. The analytical column temperature was set at 55 °C during the experiments. The mobile phase and elution gradient used for peptide separation were as follows: 0.1% formic acid in water as buffer A and 0.1% formic acid in 80% acetonitrile as buffer B, 0–1 min, 6–10% B; 1–96 min, 10–36% B; 96–107 min, 36–60% B; 107–108 min, 60–100% B; 108–120 min, 100% B. The flow rate was set as 300 nl min^{-1}.

Data-dependent tandem mass spectrometry (MS/MS) analysis was performed with a Q Exactive Orbitrap mass spectrometer (Thermo Fisher Scientific). Peptides eluted from the LC column were directly electrosprayed into the mass spectrometer with the application of a distal 2.2-kV spray voltage. A cycle of one full-scan MS spectrum (m/z 300–1,800) was acquired, followed by top 20 MS/MS events sequentially generated on the first to the twentieth most intense ions selected from the full MS spectrum at a 28% normalized collision energy. Full-scan resolution was set to 70,000 with an automated gain control (AGC) target of 3e6. MS/MS scan resolution was set to 17,500 with an isolation window of 1.8 m/z and an AGC target of 1×10^{-5}. The number of micro scans was one for both MS and MS/MS scans, and the maximum ion injection time was 50 ms and 100 ms, respectively. The dynamic exclusion settings used were as follows: charge exclusion, 1, 2, 8 and >8; exclude isotopes, on; and exclusion duration, 5, 10 or 15 s. MS scan functions and LC solvent gradients were controlled by the Xcalibur data system (Thermo Fisher Scientific). Peptides containing the isopeptide bonds were identified using pLink2 software (pFind Team) as described previously[37,38]. Search parameters in pLink were: enzyme: trypsin; missed cleavages: 3; precursor and fragment tolerance: 20 ppm. Carbamidomethylation of cysteine was set as a fixed modification, and oxidation of methionine was set as a variable modification. The results were filtered by applying a 5% false-discovery-rate cut-off at the spectral level.

END-seq

Sequencing reactions were performed in a 35 μl volume of cleavage buffer (50 mM HEPES, pH 7.5, 30 mM KCl, 2 mM DTT and 1 mM $MgCl_2$) containing 5 nM plasmid substrate with 400 nM wild-type or Y138F protein complex. The reactions were incubated for 60 min at 37 °C, then terminated by adding 0.5 μl of 500 mM EDTA and 0.8 μl of proteinase K (Roche, 20 mg ml^{-1}), followed by an incubation for 30 min at 55 °C. NaCl was subsequently added to a final concentration of 150 mM. END-seq was performed as previously described, with modifications[39]. In brief, 12.5-day-old mouse testicular cells were washed twice in ice-cold PBS and resuspended in ice-cold cell suspension buffer. After equilibration at room temperature for 5 min, the resuspended testicular cells were combined with the cleavage reaction and embedded in 0.75% agarose (final concentration), solidifying at 4 °C for 15 min. The embedded cells were then lysed and digested with proteinase K (50 °C for 1 h, then 37 °C for 7 h). After washes with TE buffer (Tris-EDTA, pH 8.0), the plugs were treated with RNase at 37 °C for 1 h, followed by digestion with exonuclease VII (NEB) at 37 °C for 1 h and exonuclease T (NEB) at 24 °C for 45 min to blunt the DNA ends. After blunting, A-tails were added to the free 3′-OH ends, which were then ligated with END-seq hairpin adaptor 1. The agarose plugs were subsequently melted and dialysed, and the released DNA was sonicated to achieve DNA fragments of about 170 bp in length. These DNA fragments were collected and purified, then dissolved in 70 μl TE buffer. Biotinylated adaptor 1-DNA fragments were further isolated using MyOne streptavidin beads. The second end was repaired and A-tails were added, followed by ligation with END-seq hairpin adaptor 2. Both hairpin ends were digested with USER (NEB), and the resulting DNA fragments were amplified by PCR. The libraries were then sequenced using the Illumina HiSeq 2000 platform.

END-seq data analysis

Read1 reads were aligned to the mouse (GRCm38p2/mm10 plus plasmid) genome using Bowtie (v.1.2.1.1)[40], allowing three mismatches and retaining only the best strata for reads with multiple alignments (-n 3 -k 1 -l 50). The 'view' and 'sort' functions in SAMtools (v.1.9) were used to convert and sort the mapping output, generating sorted BAM files[41]. BAM files were further converted to BED files using the bedtools (v.2.25.0) 'bamtobed' command[42]. To normalize read density (reads per million), the 'genomecov' function in bedtools (v.2.25.0) was applied, followed by conversion to a .bw file. Break positions were identified using the 5′ end of the reads.

Histological and immunohistochemical analyses

Testes from 19-dpp mice or ovaries from 12-dpp mice were fixed in either Bouin's solution at room temperature or 4% paraformaldehyde (PFA) at 4 °C overnight, followed by embedding in paraffin and sectioning at a thickness of 5 μm. The sections fixed in Bouin's solution were deparaffinized, rehydrated and stained with haematoxylin and eosin (H&E) for histological analysis. Each mouse was randomly selected on the basis of genotype, and the genotype was unknown during the analysis of fluorescent signals to ensure blinding. For immunofluorescence analysis, sections fixed in PFA were subjected to antigen retrieval by boiling in antigen retrieval buffer (10 mM sodium citrate, pH 6.0) for 18 min in a microwave oven, followed by cooling on ice for 30 min. Sections were then washed in PBS containing 0.1% Triton X-100 (PBST) and incubated in blocking buffer (10% donkey serum, 1% BSA in PBST) for 60 min at room temperature. Then the sections were incubated overnight at room temperature with rabbit anti-MVH (1:200, Abcam) in a blocking buffer. After washing in PBST, the slides were incubated with Alexa Fluor 594-conjugated donkey anti-mouse secondary antibody (1:500, Jackson ImmunoResearch) for 60 min at room temperature. After further washes in PBST, sections were mounted in Prolong Gold Antifade medium with DAPI (Molecular Probes) and imaged using a fluorescence microscope (Zeiss, Axio Scope A1) by Zen capture software (Zeiss, v.2.3 blue edition).

Spermatocyte chromosome spreading and immunofluorescence staining

Testes were collected from 19-dpp male mice for spermatocyte chromosome spreading[43]. Each mouse was randomly selected on the basis

of genotype, and the genotype was unknown during the analysis of fluorescent signals to ensure blinding. In brief, seminiferous tubules were treated with hypotonic buffer (30 mM Tris, 5 mM EDTA, 50 mM sucrose, 17 mM trisodium citrate dihydrate and 0.5 mM dithiothreitol, pH 8.2) for 10–20 min, followed by gentle smashing in 100 mM sucrose buffer (pH 8.2). The resulting suspension was gently spread onto slides pre-coated with fixative buffer (1% PFA, 0.15% Triton X-100, pH 9.2) and air-dried in a humidity chamber at room temperature. After washing in PBST, the slides were incubated in blocking buffer (10% donkey serum, 1% BSA in PBST) for 60 min at room temperature. Then, the slides were incubated overnight at room temperature using the following primary antibodies: mouse anti-γH2AX (1:500, Millipore), mouse anti-SYCP3 (1:200, Santa Cruz), rabbit anti-SYCP3 (1:200, Abcam), rabbit anti-SYCP1 (1:200, Abcam) and rabbit anti-RPA2 (1:200; a gift from M. Luo). After washing in PBST, the slides were incubated for 60 min at room temperature with the following secondary antibodies: Alexa Fluor 488-conjugated donkey anti-mouse IgG (1:500, Jackson ImmunoResearch), Alexa Fluor 594-conjugated donkey anti-mouse IgG (1:500, Jackson ImmunoResearch), Alexa Fluor 488-conjugated donkey anti-rabbit IgG (1:500, Jackson ImmunoResearch) and Alexa Fluor 488-conjugated donkey anti-rabbit IgG (1:500, Jackson ImmunoResearch). After incubation with the corresponding secondary antibodies and washing in PBST, slides were mounted in Prolong Gold Antifade medium with DAPI (Molecular Probes) and imaged with a fluorescence microscope (Zeiss, Axio Scope A1) by Zen capture software (Zeiss, v.2.3 blue edition). For the quantification of γH2AX intensity, matched-exposure images were taken and signal intensities were measured by ImageJ.

Structural prediction using AlphaFold 3

AlphaFold 3 was used to predict the structures of the SPO11–TOP6BL heterodimer, the SPO11–TOP6BL tetramer and the SPO11–TOP6BL tetramer in complex with DNA[44]. The predicted three-dimensional structures were visualized using PyMOL software for detailed structural analysis[44].

Statistics and reproducibility

A Mann–Whitney *U* test was used to evaluate the statistical significance of RPA foci or γH2AX intensity per cell between controls and mutants. *P* values were calculated using GraphPad Prism v.10. Time courses of linear DNA formation were fitted to an allosteric sigmoidal model in Prism v.10. The statistical significance of comparisons between wild-type and mutant SPO11 was assessed using a two-way ANOVA. For EMSA, binding curves were fitted individually with GraphPad Prism v.10 software, using a dose response that incorporated a Hill slope. Data were normalized to reflect the percentage of bound oligonucleotides and are presented as the mean ± s.d. of the interpolated K_d from three independent experiments. Each conclusion in the manuscript was based on results that were reproduced in at least three independent experiments and at least three mice of each genotype.

Reporting summary

Further information on research design is available in the Nature Portfolio Reporting Summary linked to this article.

Data availability

The XL-MS raw data and peak search results generated in this study have been deposited to the ProteomeXchange Consortium (https://proteomecentral.proteomexchange.org) via the iProX partner repository with the dataset identifier PXD058354. The END-seq data generated in this study have been deposited to the Gene Expression Omnibus (https://www.ncbi.nlm.nih.gov/geo) with the accession number GSE281557.

37. Lu, S. et al. Mapping native disulfide bonds at a proteome scale. *Nat. Methods* **12**, 329–331 (2015).
38. Yang, B. et al. Identification of cross-linked peptides from complex samples. *Nat. Methods* **9**, 904–906 (2012).
39. Liu, Y., Lin, Z., Yan, J., Zhang, X. & Tong, M.-H. A *Rad50*-null mutation in mouse germ cells causes reduced DSB formation, abnormal DSB end resection and complete loss of germ cells. *Development* **151**, dev202312 (2024).
40. Langmead, B., Trapnell, C., Pop, M. & Salzberg, S. L. Ultrafast and memory-efficient alignment of short DNA sequences to the human genome. *Genome Biol.* **10**, R25 (2009).
41. Li, H. et al. The Sequence Alignment/Map format and SAMtools. *Bioinformatics* **25**, 2078–2079 (2009).
42. Quinlan, A. R. & Hall, I. M. BEDTools: a flexible suite of utilities for comparing genomic features. *Bioinformatics* **26**, 841–842 (2010).
43. Peters, A. H., Plug, A. W., van Vugt, M. J. & de Boer, P. A drying-down technique for the spreading of mammalian meiocytes from the male and female germline. *Chromosome Res.* **5**, 66–68 (1997).
44. Abramson, J. et al. Accurate structure prediction of biomolecular interactions with AlphaFold 3. *Nature* **630**, 493–500 (2024).

Acknowledgements We thank D. Li, J. Ding and G. Cai for experimental support, and M. Luo for providing an anti-RPA2 antibody. This work was supported by grants from the National Key R&D Program of China (2022YFC2702602 and 2021YFC2700200 to M.-H.T.; 2022YFA1103900 to W.W.), the National Natural Science Foundation of China (31930034 to M.-H.T.; 32171186 and 91940302 to Y.H.; and 32370575 to W.W.), the Strategic Priority Research Program of the Chinese Academy of Sciences (XDB0980000 to W.W.) and the Chinese Academy of Sciences (318GJHZ2023004MI to W.W.). We acknowledge the Vivarium services at CEMCS (Center for Excellence in Molecular Cell Sciences). We are grateful to the National Facility for Protein Science in Shanghai for facilitating the collection of mass-spectrometry data.

Author contributions M.-H.T. conceived the project. M.-H.T., Y.H. and J.M. designed the project and the data analysis. M.-H.T., Y.H., X.T. and Z.H. wrote the manuscript with contributions from all authors. X.T. generated expression vectors, purified proteins and reconstituted the meiotic DSB formation. Z.H. performed EMSAs, expression and purification of human TDP2, pull-downs, co-immunoprecipitation, cross-linking and fluorescent oligo cleavage. J.D. did the initial expression and purification of the Spo11 complex. M.W. performed mouse phenotypic analyses, including histological analyses and spermatocyte chromosome spreading with immunofluorescence staining. P.G. performed END-seq experiments. Y.S. and W.W. analysed and interpreted the END-seq data. Y.Y. performed XL-MS analyses.

Competing interests The authors declare no competing interests.

Additional information

Supplementary information The online version contains supplementary material available at https://doi.org/10.1038/s41586-024-08551-1.

Correspondence and requests for materials should be addressed to Ying Huang or Ming-Han Tong.

Peer review information *Nature* thanks Liangran Zhang and the other, anonymous, reviewer(s) for their contribution to the peer review of this work.

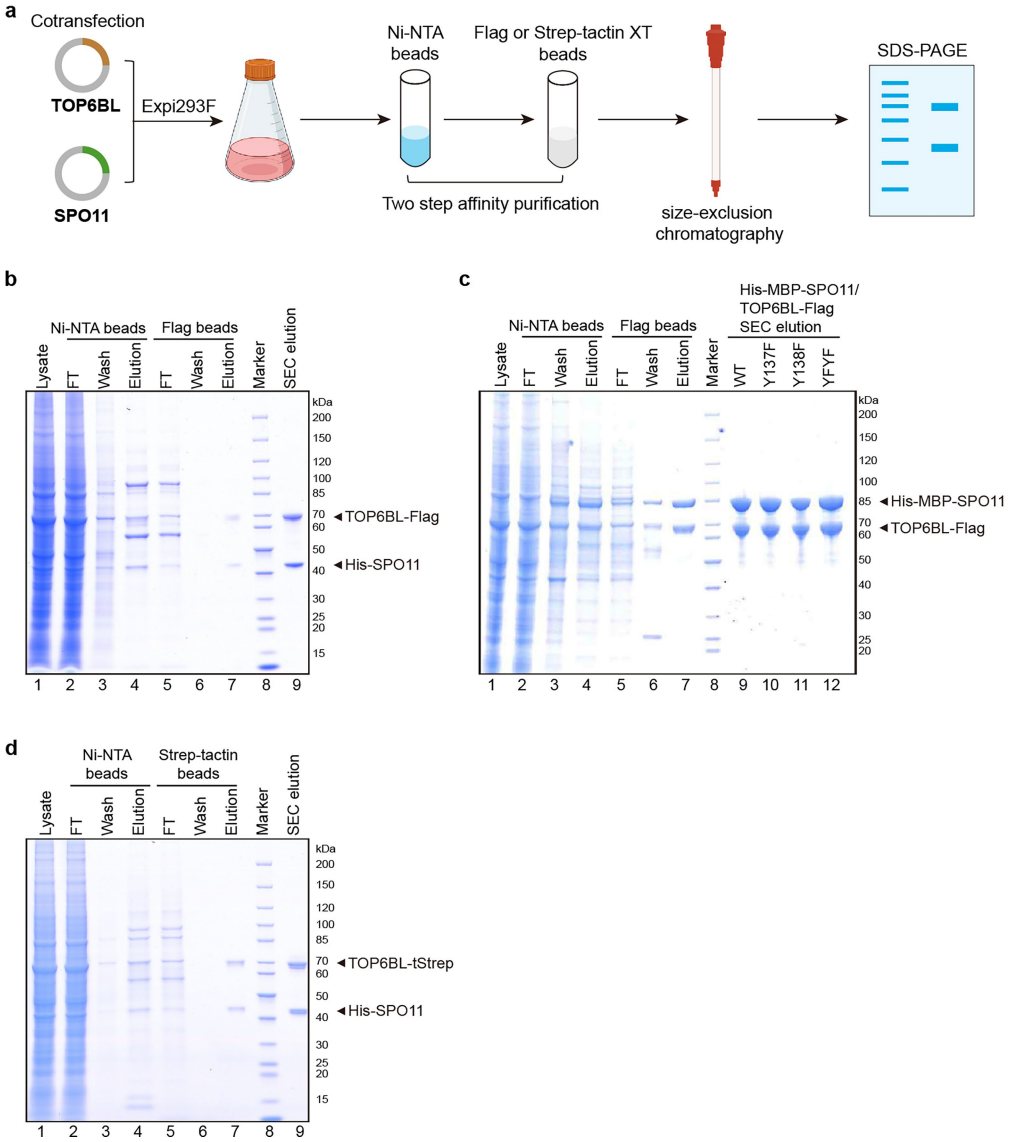

Extended Data Fig. 1 | Purification of SPO11–TOP6BL complexes. a, Schematic representation of the purification process for SPO11–TOP6BL complexes. Image of triangle bottle was created in BioRender (https://BioRender.com/a10w137). Image of chromatographic column was created in Figdraw (https://www.figdraw.com). **b**–**d**, SDS–PAGE analysis illustrating the purification process of SPO11–TOP6BL complexes, including His–SPO11/TOP6BL–Flag in (**b**), His–MBP–SPO11/TOP6BL/Flag in (**c**), and His–SPO11/TOP6BL–tStrep in (**d**) (n = 3 independent experiments).

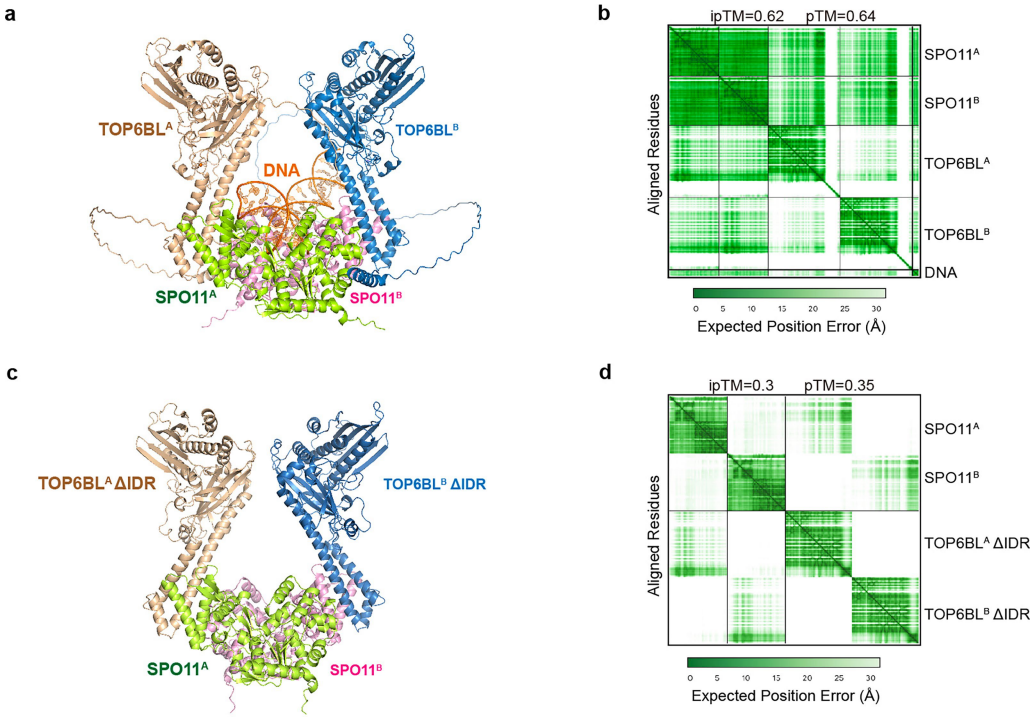

Extended Data Fig. 2 | Structural characteristics of TOP6BL predicted by AlphaFold 3. a,**c**, Cartoon representation of full-length SPO11–TOP6BL (**a**) and the TOP6BL ΔIDR variant (**c**) as predicted by AlphaFold 3. **b**,**d**, PAE plot along with ipTM and pTM scores that assess the accuracy of the structural model shown in **a** and **c**, respectively, providing insight into the model's reliability and the confidence levels of the predicted atomic positions.

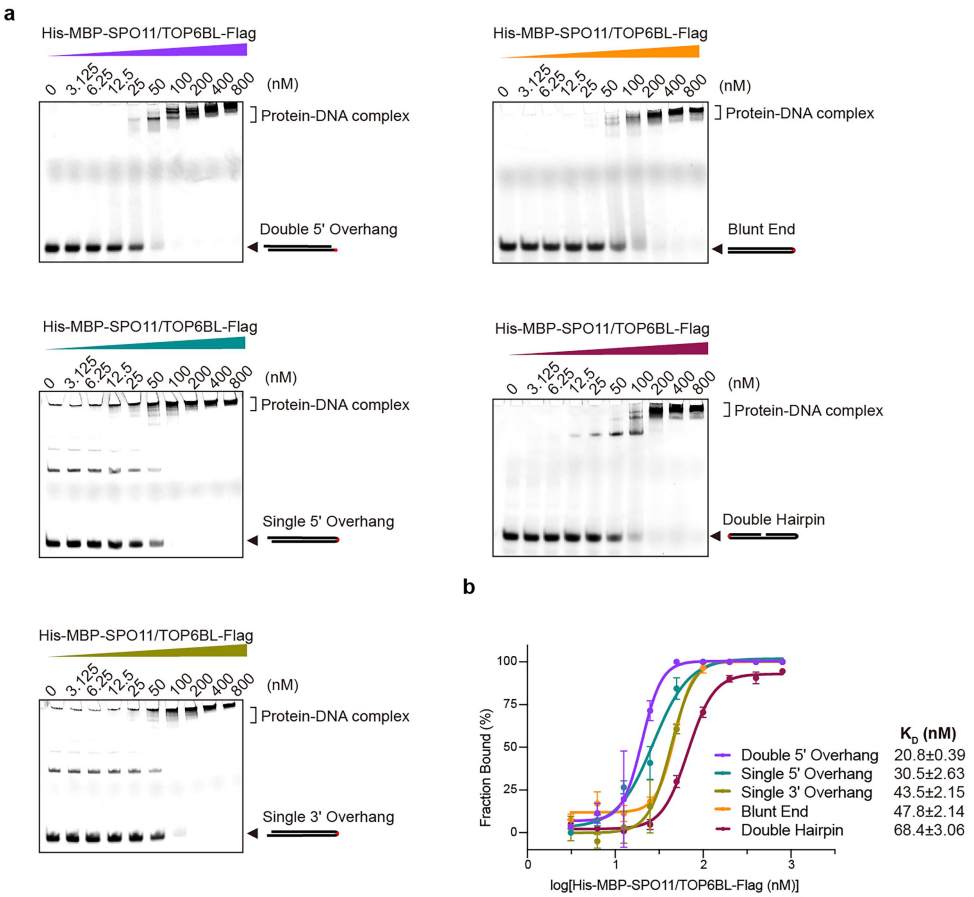

Extended Data Fig. 3 | Binding of SPO11–TOP6BL to oligonucleotides with different overhang structures. a, EMSA experiments assessed the binding affinity of MBP–SPO11–TOP6BL to five distinct DNA oligonucleotides: a dsDNA with 2-nt 5′ overhangs on both ends (top left), a 2-nt 5′ overhang hairpin (middle left), a 2-nt 3′ overhang hairpin (bottom left), a blunt-end hairpin (top right), and a double hairpin (nicked; middle right). **b**, A binding affinity curve was generated from the EMSA results in **a**, depicting the fraction bound (%) versus the concentration of the SPO11–TOP6BL complex (n = 3 independent experiments; mean ± s.d.).

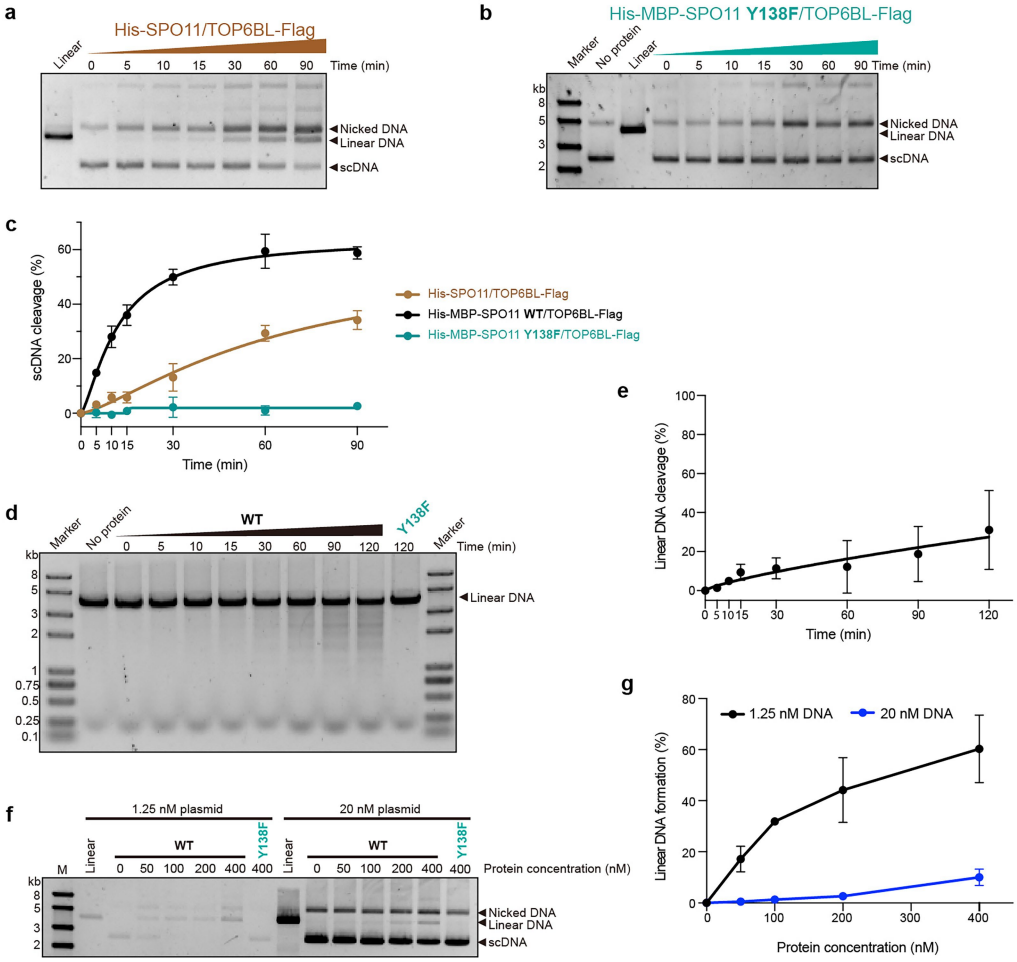

Extended Data Fig. 4 | Kinetics of the SPO11–TOP6BL complex in DNA cleavage. a,**b**, Time course of the cleavage assay conducted on plasmid DNA by the His–SPO11/TOP6BL–Flag (**a**) and His–MBP–SPO11 Y138F/TOP6BL–Flag (n = 3 independent experiments) (**b**) complexes at various time points. **c**, Diagram illustrating the kinetics of plasmid DNA cleavage over time by SPO11–TOP6BL complexes (n = 3 independent experiments; mean ± s.d.). **d**, Linear DNA cleavage by His–SPO11/TOP6BL–Flag under Mg^{2+} over time. **e**, Diagram illustrating the kinetics of linear DNA cleavage over time by SPO11–TOP6BL complexes (n = 3 independent experiments; mean ± s.d.). **f**, Titration of protein concentration over different plasmid DNA concentrations as measured by plasmid DNA cleavage. **g**, Quantification of plasmid DNA cleavage from **f** (n = 3 independent experiments; mean ± s.d.). Because plasmid DNA concentrations were not constant, greyscale values were normalized by dividing by the highest cleavage signal observed in each experiment.

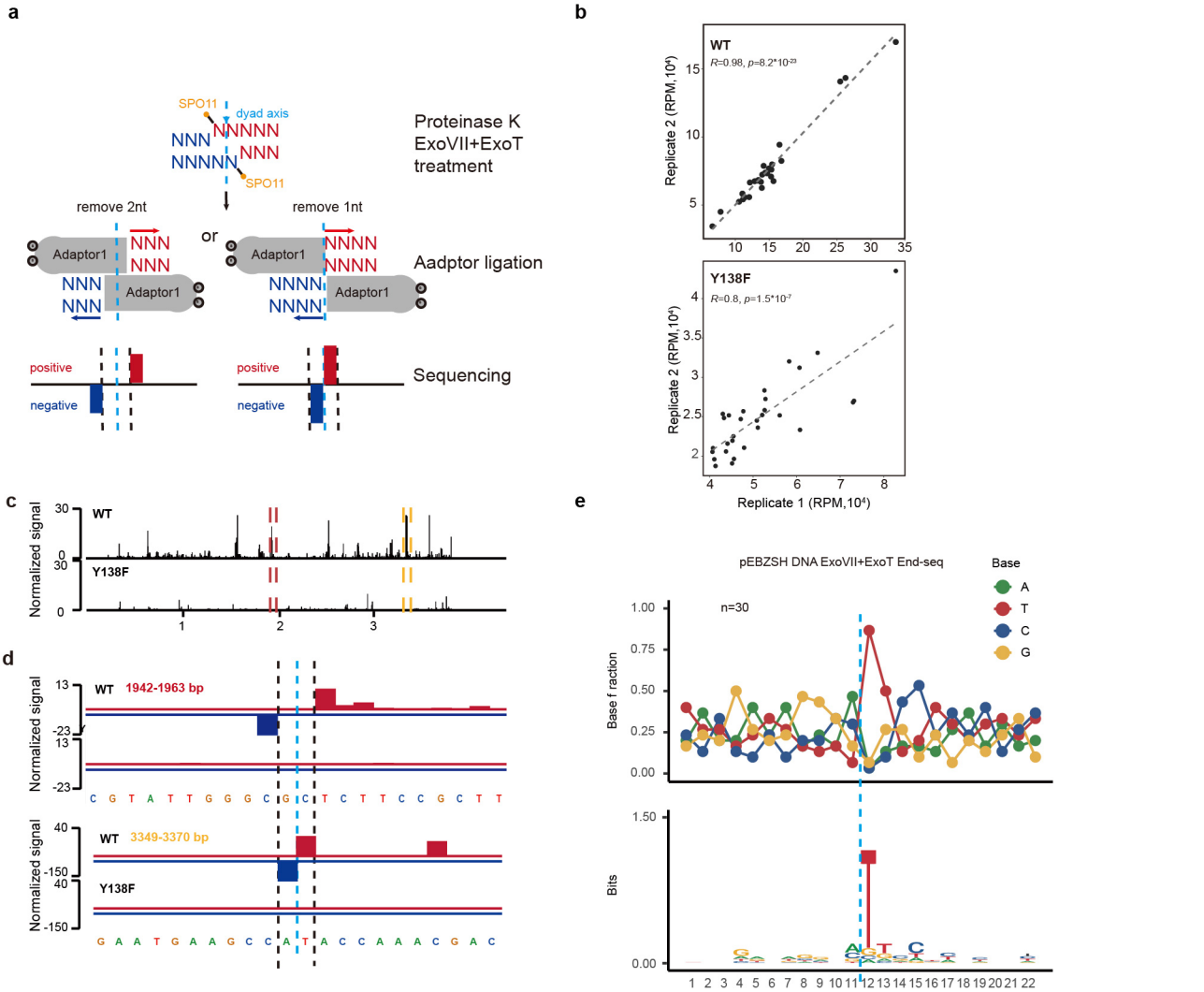

Extended Data Fig. 5 | Analysis of cleavage sequence preferences by the SPO11 complex. a, Schematic of END-seq. SPO11 cleavage products are expected to have a 2-nt 5′ overhang. Because ExoVII cannot efficiently excise short (≤4 bp) ssDNA, SPO11 cleavage products are mainly processed into two types, resulting in two main patterns. **b**, Correlation between replicate END-seq datasets for in vitro cleavage of pEBZSH with either the SPO11–TOP6BL (wild-type, WT) (top) or the Y138F-mutant (bottom) complexes. Pearson correlation coefficients and *P* values are indicated (two-sided). **c**, END-seq of in vitro cleavage reactions on pEBZSH DNA with either WT (top) or Y138F-mutant (bottom) complexes. **d**, Detailed view of **c**, with the blue dashed line indicating the dyad axis of preferred cleavage sites. **e**, Base composition bias around in vitro cleavage sites, showing the fractional base composition (top) and sequence logo (bottom).

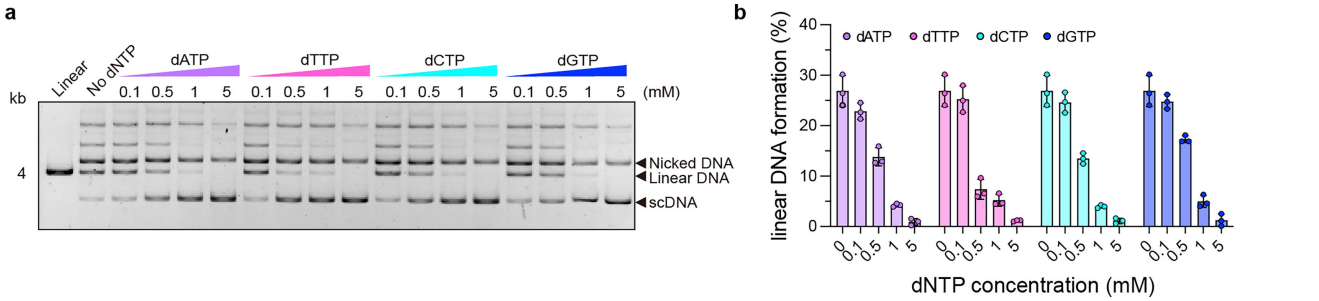

Extended Data Fig. 6 | Inhibitory effects of dNTPs on MBP–SPO11–TOP6BL cleavage activity. a, Analysis of the effect of dNTPs on the plasmid-cleaving activity of the MBP–SPO11–TOP6BL complex. The addition of dATP, dTTP, dCTP, and dGTP does not augment the cleavage activity; rather, these nucleotides exhibit concentration-dependent inhibitory effects on the enzymatic function. **b**, Bar graph providing a statistical overview of the inhibitory effect of different dNTPs on plasmid cleavage activity, as quantified in **a** (n = 3 independent experiments; mean ± s.d.).

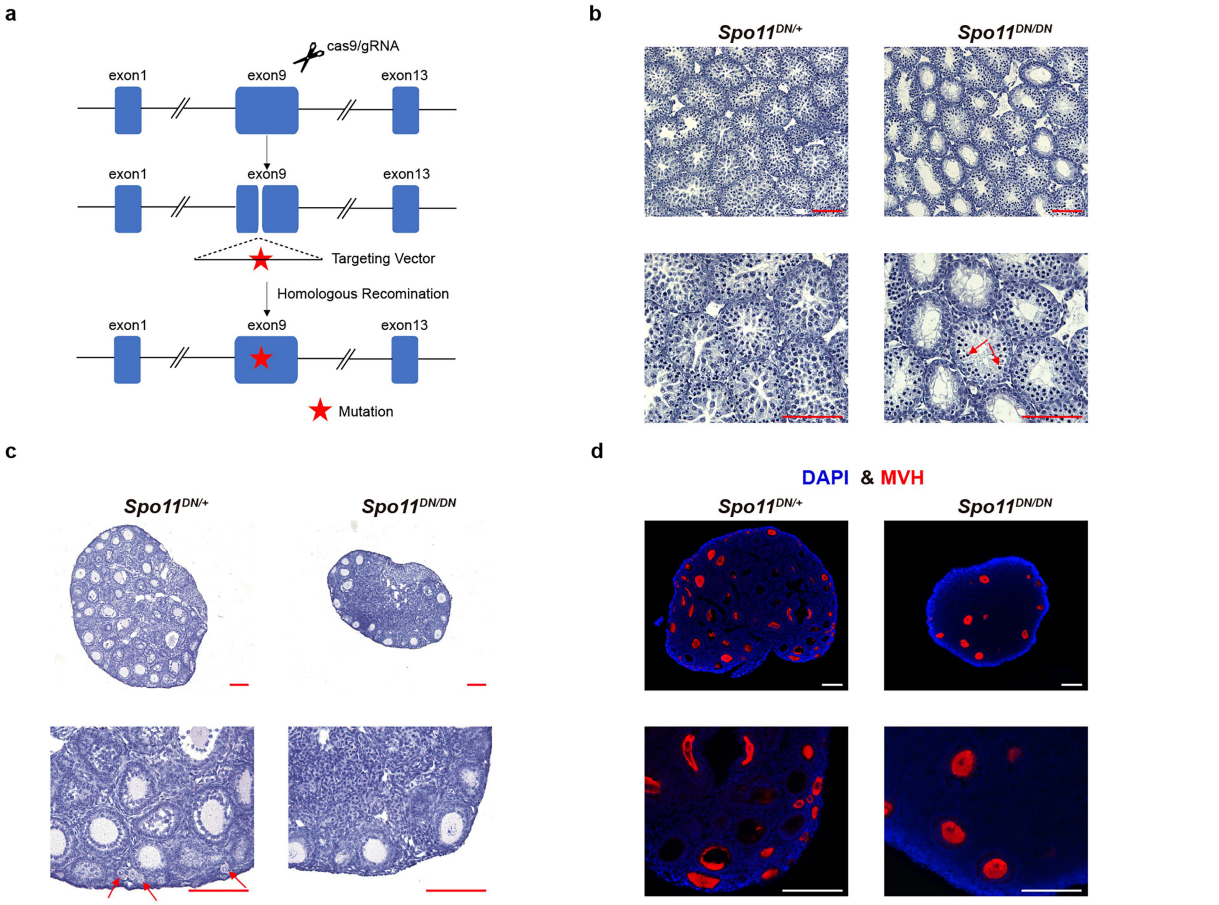

Extended Data Fig. 7 | Histological analysis of testes and ovaries from *Spo11*$^{DN/+}$ and *Spo11*$^{DN/DN}$ mice. a, Schematic diagram for the *Spo11*^{DN} mutant allele. **b**, H&E staining of testicular sections from 19-dpp control (*Spo11*$^{DN/+}$) and *Spo11*$^{DN/DN}$ mutant mice. Higher magnifications are shown below. The red arrows indicate apoptotic spermatocytes in *Spo11*$^{DN/DN}$ mutant seminiferous epithelium. (n = 3 mice, scale bars: 10 μm). **c**, H&E staining of ovary sections from 12-dpp control and *Spo11*$^{DN/DN}$ mutant mice. Higher magnifications are shown below. Red arrows indicate the primordial follicles that are absent in *Spo11*$^{DN/DN}$ ovary. (n = 3 mice, scale bars: 10 μm). **d**, Immunofluorescence staining for MVH (red, germ cell marker) in 12-dpp control and *Spo11*$^{DN/DN}$ mutant ovary sections. Higher magnifications are shown below. (n = 3 mice, scale bars: 10 μm).

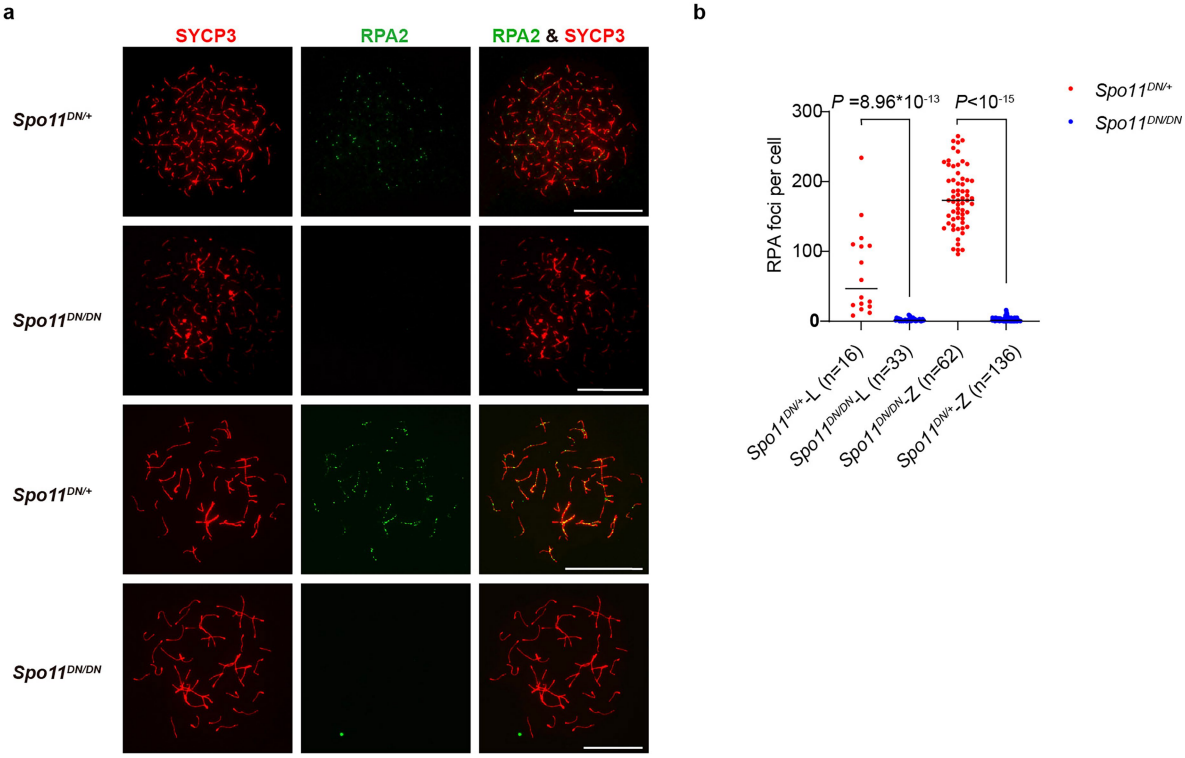

Extended Data Fig. 8 | Meiotic recombination is impaired in *Spo11*$^{DN/DN}$ mutant spermatocytes. a, RPA2 (green) and SYCP3 (red) were detected on chromosome spreads of spermatocyte from control (*Spo11*$^{DN/+}$) and *Spo11*$^{DN/DN}$ mutant mice (scale bars: 10 µm). **b**, Quantification of RPA2 foci in leptotene (L) and early zygotene (Z) spermatocytes in control mice and *Spo11*$^{DN/DN}$ mutants. *n* indicates the numbers of cells analysed from three (control) and four (*Spo11*$^{DN/DN}$ mutant) pooled experiments, respectively. *P* values were calculated using the Mann–Whitney test (two-sided), and median focus numbers are indicated. No RPA2 foci were detected in *Spo11*$^{DN/DN}$ mutant spermatocytes. The original data of nuclear spreads can be found in Supplementary Data.

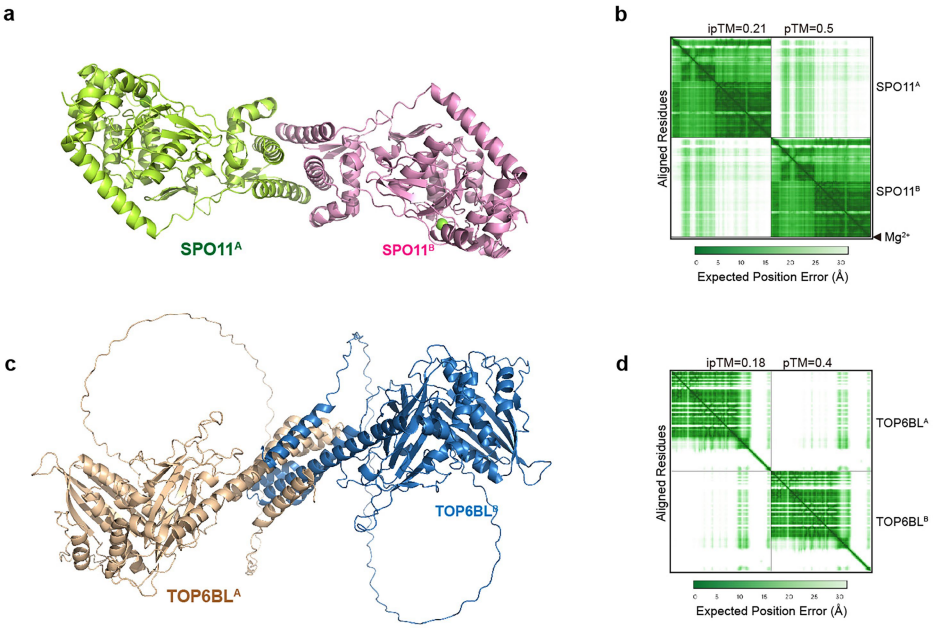

Extended Data Fig. 9 | AlphaFold 3-predicted SPO11 and TOP6BL homodimers. a,**c**, Cartoon representation of the predicted SPO11–SPO11 (**a**) and TOP6BL–TOP6BL (**c**) homodimers, as modelled by AlphaFold 3. **b**,**d**, PAE plot along with ipTM and pTM scores that assess the accuracy of the structural model shown in **a** and **c**, respectively, providing insight into the model's reliability and the confidence levels of the predicted atomic positions.

nature portfolio

Corresponding author(s): Ying Huang, Ming-han Tong

Last updated by author(s): Nov 9, 2024

Reporting Summary

Nature Portfolio wishes to improve the reproducibility of the work that we publish. This form provides structure for consistency and transparency in reporting. For further information on Nature Portfolio policies, see our Editorial Policies and the Editorial Policy Checklist.

Statistics

For all statistical analyses, confirm that the following items are present in the figure legend, table legend, main text, or Methods section.

n/a	Confirmed	
☐	☒	The exact sample size (*n*) for each experimental group/condition, given as a discrete number and unit of measurement
☐	☒	A statement on whether measurements were taken from distinct samples or whether the same sample was measured repeatedly
☐	☒	The statistical test(s) used AND whether they are one- or two-sided *Only common tests should be described solely by name; describe more complex techniques in the Methods section.*
☒	☐	A description of all covariates tested
☒	☐	A description of any assumptions or corrections, such as tests of normality and adjustment for multiple comparisons
☐	☒	A full description of the statistical parameters including central tendency (e.g. means) or other basic estimates (e.g. regression coefficient) AND variation (e.g. standard deviation) or associated estimates of uncertainty (e.g. confidence intervals)
☐	☒	For null hypothesis testing, the test statistic (e.g. *F*, *t*, *r*) with confidence intervals, effect sizes, degrees of freedom and *P* value noted *Give P values as exact values whenever suitable.*
☒	☐	For Bayesian analysis, information on the choice of priors and Markov chain Monte Carlo settings
☒	☐	For hierarchical and complex designs, identification of the appropriate level for tests and full reporting of outcomes
☐	☒	Estimates of effect sizes (e.g. Cohen's *d*, Pearson's *r*), indicating how they were calculated

Our web collection on statistics for biologists contains articles on many of the points above.

Software and code

Policy information about availability of computer code

Data collection	We used commercial software, available as a package with the respective instrument, for data collection. This includes Typhoon FLA 9000 capture software (GE Healthcare, Version 1.0), Zen capture software (Zeiss, Version 2.3 blue edition), Tanon MP software (Tanon, Version 1.0). XL-MS data were collected using Q Exactive Orbitrap mass spectrometer (Thermo Scientific). The data was demultiplexed using bcl2fastq v2.20 software from Illumina.
Data analysis	Only commercial or publicly available software was used for data analysis. This includes image J (NIH, Version 1.53k) for the analysis of gel data; graphs and numerical data (including statistics/error bars) was analyzed and plotted by Prim (GraphPad, Version 10.0); Peptides containing the isopeptide bonds were identified using pLink (Version 2.0). END-seq data were analyzed bowtie (Version 1.2.1.1), samtools (Version 1.9), bedtools (v2.25.0). Sequence Alignment of SPO11 and TOP6BL were conducted using Clustal W within the JalView software (Version 2.11.4.1) and were manually refined based on structural alignment performed by Foldseek on the web (search.foldseek.com/search). The construct sequence of SPO11 and TOP6BL were exported from snapgene software (Version 8.0, www.snapgene.com).

For manuscripts utilizing custom algorithms or software that are central to the research but not yet described in published literature, software must be made available to editors and reviewers. We strongly encourage code deposition in a community repository (e.g. GitHub). See the Nature Portfolio guidelines for submitting code & software for further information.

Data

Policy information about availability of data

All manuscripts must include a data availability statement. This statement should provide the following information, where applicable:

- Accession codes, unique identifiers, or web links for publicly available datasets
- A description of any restrictions on data availability
- For clinical datasets or third party data, please ensure that the statement adheres to our policy

The cross-linking mass spectrometry raw data and peak search results generated in this study have been deposited to the ProteomeXchange Consortium (https://proteomecentral.proteomexchange.org) via the iProX partner repository with the dataset identifier PXD058354. The END-seq data generated in this study have been deposited to the Gene Expression Omnibus (https://www.ncbi.nlm.nih.gov/geo, GEO accession: GSE281557). The mouse reference genome was used for END-seq (GRCm38 - mm10).

Research involving human participants, their data, or biological material

Policy information about studies with human participants or human data. See also policy information about sex, gender (identity/presentation), and sexual orientation and race, ethnicity and racism.

Reporting on sex and gender	no applicable
Reporting on race, ethnicity, or other socially relevant groupings	no applicable
Population characteristics	no applicable
Recruitment	no applicable
Ethics oversight	no applicable

Note that full information on the approval of the study protocol must also be provided in the manuscript.

Field-specific reporting

Please select the one below that is the best fit for your research. If you are not sure, read the appropriate sections before making your selection.

☒ Life sciences ☐ Behavioural & social sciences ☐ Ecological, evolutionary & environmental sciences

For a reference copy of the document with all sections, see nature.com/documents/nr-reporting-summary-flat.pdf

Life sciences study design

All studies must disclose on these points even when the disclosure is negative.

Sample size	Sample size (or number of repeats) was chosen based on what is common in the field, and what was practical to do.(Elda Canavo, et al., nature, doi: 10.1038/s41586-020-2592-2; Alexandre Nore, et al., Nature Communication, doi: 10.1038/s41467-022-34799-0.)
Data exclusions	In general, no data were excluded unless there was a valid reason to do so, e.g. experiments with failed positive controls indicating technical problems, or when loading control indicated unequal loading that invalidated the analysis or other technical issues (broken gels, collapsed wells in gels etc.).
Replication	All biochemical experiments were performed at least three times, as defined in Figure legends. Experiments that could not be reproduced are not presented in this study.
Randomization	For animal assays, the mice were randomly taken out from cages.
Blinding	For RPA2 foci and γH2AX intensity analysis, the investigators were blinded to group allocation during data analysis.

Reporting for specific materials, systems and methods

We require information from authors about some types of materials, experimental systems and methods used in many studies. Here, indicate whether each material, system or method listed is relevant to your study. If you are not sure if a list item applies to your research, read the appropriate section before selecting a response.

Materials & experimental systems

n/a	Involved in the study
☐	☒ Antibodies
☐	☒ Eukaryotic cell lines
☒	☐ Palaeontology and archaeology
☐	☒ Animals and other organisms
☒	☐ Clinical data
☒	☐ Dual use research of concern
☒	☐ Plants

Methods

n/a	Involved in the study
☒	☐ ChIP-seq
☒	☐ Flow cytometry
☒	☐ MRI-based neuroimaging

Antibodies

Antibodies used

For immunofluorescence, primary antibodies used were mouse anti-SYCP3 (1:200 dilution; Santa Cruz, sc-74568), rabbit anti-SYCP1 (1:200, Abcam, ab15090), rabbit anti-RPA2 (1:200 dilution; gift from professor Mengcheng Luo, Wuhan University), mouse anti-γH2AX (1:500 dilution; Millipore, 5636) and ribbit anti-MVH (1:200 dilution; abcam, ab13840).Secondary antibodies used were Alexa Fluor® 594 AffiniPure™ Donkey Anti-Rabbit IgG (H+L) (1:500 dilution; Jackson ImmunoResearch, 711-585-152), Alexa Fluor® 594 AffiniPure™ Donkey Anti-Mouse IgG (H+L) (1:500 dilution; Jackson ImmunoResearch, 711-585-151) and Alexa Fluor® 488 AffiniPure™ Donkey Anti-Mouse IgG (H+L) (1:500 dilution; Jackson ImmunoResearch, 711-545-151).
For western blot, primary antibodies used were His Tag Mouse Monoclonal Antibody (1:2000, HRP Conjugated, AF2879-50μL, clone name: BC11 Beyotime,), Strep II Tag Mouse Monoclonal Antibody (1:2000 dilution; HRP Conjugated, AF2927, clone name: 11D6, Beyotime), Flag Tag Mouse Monoclonal Antibody (1:2000 dilution; HRP Conjugated, AF2855-50μL, clone name: 2E6, Beyotime), MBP Tag Mouse Monoclonal Antibody (1:2000 dilution; HRP Conjugated, AF2915, clone name 1A9, Beyotime).

Validation

All commercial antibody have been frequently used in previous studies and their specificity for use in mouse is well established. The anti-RPA2 antibody was previously validated in study of Luo laboratory (Wu et al., 2021, DOI: 10.3389/fcell.2021.715733. eCollection 2021.). Validation for anti-SYCP3 antibody is available at https://www.scbt.com/zh/p/scp-3-antibody-g-3. Validation for anti-SYCP1 is available at https://www.abcam.cn/products/primary-antibodies/scp1-antibody-ab15090.html. Validation for anti-MVH is available at https://www.abcam.cn/products/primary-antibodies/ddx4--mvh-antibody-ab13840.html. Validation for His Tag Mouse Monoclonal Antibody is available at https://www.beyotime.com/product/AF2879-50%CE%BCl.htm. Validation for Strep II Tag Mouse Monoclonal Antibody is available at https://www.beyotime.com/product/AF2927.htm. Flag Tag Mouse Monoclonal Antibody is available at https://www.beyotime.com/product/AF2855-50%CE%BCl.htm. MBP Tag Mouse Monoclonal Antibody is available at https://www.beyotime.com/product/AF2915.htm.

Eukaryotic cell lines

Policy information about cell lines and Sex and Gender in Research

Cell line source(s)	Expi293F cells were kindly provided by Cell Bank, Chinese Academy of Sciences.
Authentication	Cell lines were not authenticated.
Mycoplasma contamination	Cell lines were not verified to be free of mycoplasma contamination.
Commonly misidentified lines (See ICLAC register)	No commonly misidentified species used.

Animals and other research organisms

Policy information about studies involving animals; ARRIVE guidelines recommended for reporting animal research, and Sex and Gender in Research

Laboratory animals	Mice were fed regular rodent chow with ad libitum access water and food in 12-hour light-dark cycle in a temperature and humidity-controlled environment (20-26°C, 30-70% humidity) . Euthanasia was by CO2 asphyxiation. The Spo11 D277N mouse line was generated by Shanghai Biomodel Organism Co., Ltd using the CRISPR/Cas9 technology. The donor oligos were designed to change the D277 codon GAT (D) to AAT (N). The resulting point-mutation founders were backcrossed with adult C57BL/6J mice (WT; from Shanghai Biomodel Organism Co., Ltd) to obtain heterozygous mutant animals. Homozygous mutant mice were produced by self fertilization of heterozygous. 12 dpp female mice and 19 dpp male mice were used for phenotypic analysis in this study.
Wild animals	This study did not involve wild animals.
Reporting on sex	We separately studied the phenotypes of Spo11 D277N mutations in males and females using the common methods in the field.
Field-collected samples	The study did not involve samples collected from the field.
Ethics oversight	The experiments performed in this study were approved by the Ethics Committee of Center for Excellence in Molecular Cell Science, Chinese Academy of Sciences (2022-088)

Note that full information on the approval of the study protocol must also be provided in the manuscript.

Plants

Seed stocks	no applicable
Novel plant genotypes	no applicable
Authentication	no applicable